

This is a postprint version of the following published document:

Iannelli, A., Lowenberg, M., & Marcos, A. (2020). Computation of Bifurcation Margins Based on Robust Control Concepts. *In SIAM Journal on Applied Dynamical Systems*, 19(3), 1956–1992.

DOI:[10.1137/19m1303678](https://doi.org/10.1137/19m1303678)

© 2020, Society for Industrial and Applied Mathematics

# COMPUTATION OF BIFURCATION MARGINS BASED ON ROBUST CONTROL CONCEPTS

ANDREA IANNELLI\*, MARK LOWENBERG †, AND ANDRÉS MARCOS†

**Abstract.** This article proposes a framework which allows the study of stability robustness of equilibria of a nonlinear system in the face of parametric uncertainties from the point of view of bifurcation theory. In this context, a branch of equilibria is stable if bifurcations (i.e. qualitative changes of the steady-state solutions) do not occur as one or more bifurcation parameters are varied. The work focuses specifically on Hopf bifurcations, where a stable branch of equilibria meets a branch of periodic solutions. It is of practical interest to evaluate how the presence of uncertain parameters in the system alters the result of analyses performed with respect to a nominal vector field. Note that in this article bifurcation parameters have a different meaning than uncertain parameters. To answer the question, the concept of robust bifurcation margins is proposed based on the idea of describing the uncertain system in a Linear Fractional Transformation fashion. The robust bifurcation margins can be interpreted as nonlinear analogs of the structural singular value, or  $\mu$ , which provides robust stability margins for linear time invariant systems. Their computation is formulated as a nonlinear program aided by a continuation-based multi-start strategy to mitigate the issue of local minima. Application of the framework is demonstrated on two case studies from the power system and aerospace literature.

**Key words.** Bifurcations, numerical continuation, robust control theory, robust stability

**AMS subject classifications.** 34C23, 34H20, 37G15, 93D09

**1. Introduction.** Bifurcation analysis studies qualitative changes in the response of a nonlinear system (e.g. number and type of steady-state solutions) when one or more parameters on which the dynamics depend are continuously varied [27, 21]. This is usually accomplished by selecting a few *bifurcation parameters*, typically equal in number to the codimension of the studied bifurcation, based on their importance for the system. This analysis approach is of recognized importance since it allows complex dynamic behaviours to be characterized and an understanding of the system to be gained. However, it does not provide indications on the robustness of the results to uncertainties in the models. Let us consider for example the presence of *uncertain parameters* allowed to vary within a prescribed range. These parameters reflect the fact that uncertainty is ubiquitous in engineering systems and at any stage of analysis (from preliminary to detailed). Unlike the bifurcation parameters, in principle they are not restricted in number (and are allowed to vary simultaneously) and their influence on the dynamics may not be known a priori. It is then important to estimate their effect, and in particular whether bifurcation points can move closer to operating points deemed safe on the basis of analyses applied to the nominal system.

The study of robustness within a dynamical systems perspective can be attempted by adopting singularity theory techniques (e.g. Lyapunov-Schmidt reduction) [18], as shown by recently published research [20, 8]. The central idea is to perform a reduction of the original dynamics to a lower dimension map, whose singularities represent transitions between qualitatively different bifurcation diagrams. Even though it is in principle possible to track these singularities without computing explicitly the reduction [8], the application of these techniques to systems with a moderately complex mathematical description and with generic number of uncertainties is not straight-

---

\*Department of Information Technology and Electrical Engineering, Swiss Federal Institute of Technology (ETH), Zürich 8092, Switzerland ([iannelli@control.ee.ethz.ch](mailto:iannelli@control.ee.ethz.ch)).

†Department of Aerospace Engineering, University of Bristol, BS8 1TR, United Kingdom ([m.lowenberg/andres.marcos@bristol.ac.uk](mailto:m.lowenberg@andres.marcos@bristol.ac.uk)).

45 forward and has not been presented in the literature yet. Moreover, this approach  
46 does not directly provide information on the *distance* from a given (nominally stable)  
47 operating point to the closest bifurcation, that is, a margin to the bifurcation. An-  
48 other approach which considers the effect of uncertainties by focussing on a reduced  
49 dimensional dynamics, namely the one on the centre manifold, is that proposed in  
50 [38]. The main difficulty resides here in the definition of appropriate initial condi-  
51 tions allowing a projection of the long term dynamics on the centre manifold which  
52 accurately incorporates the effect of uncertainties [37].

53 This article proposes a framework which provides a quantitative measure of the  
54 distance between branches of stable equilibria and of periodic oscillations in the uncer-  
55 tainty space. In other words, the onset of a Hopf bifurcation in the face of worst-case  
56 combinations of the uncertainty is formalised by means of a robust bifurcation margin.  
57 Previous works in the literature looked at the problem of computing perturbations  
58 to bifurcations. For example, in [12] an extension to multidimensional parameter  
59 spaces of standard methods for codimension-1 bifurcations is proposed. The problem  
60 of determining locally closest bifurcations is solved by introducing a normal vector  
61 to hypersurfaces of bifurcation points, and makes use of both direct and iterative  
62 methods. While the latter is limited to static bifurcations (i.e., saddle node, tran-  
63 scritical, and pitchfork), the former is in principle applicable also to the Hopf case.  
64 The direct method consists of solving the full set of equations defining the bifurcation  
65 (plus additional equations to close the problem) and, as pointed out by the authors  
66 of [12], it may be too onerous from a computational point of view. This approach  
67 was applied in [32] to the analysis of static bifurcations in flexible satellites, making a  
68 number of simplifying assumptions, e.g., no dependence of the equilibrium on the un-  
69 certainties and the system having Hamiltonian dynamics. A closely related approach,  
70 which according to their authors generalizes the method from [12], is discussed in [6].  
71 The work considers saddle-node bifurcations only, and the computation of the small-  
72 est perturbation to bifurcation is done by applying the generalized reduced-gradient  
73 method. In essence, this consists of a nonlinear optimization strategy making use of  
74 corrector and predictor steps and solving the system of equations defining the bifur-  
75 cation. However, the issue of local minima is not addressed and the same objection  
76 regarding the total dimension of the problem is envisaged for the Hopf bifurcation  
77 case (not discussed in that work). The idea of using vectors normal to a manifold of  
78 bifurcation points is also present in [16, 34] and other works from the same group,  
79 where the design of robustly stable and feasible processes is pursued.

80 The problem is studied in this article from the point of view of Linear Fractional  
81 Transformation (LFT) models and structured singular value ( $\mu$ ) analysis from ro-  
82 bust control theory [48]. These tools are well established for the analysis of linear  
83 uncertain systems, and provide an analytical answer to stability and performance  
84 problems. Even though a direct application to the nonlinear context is precluded  
85 by their inherently linear formulation, an extension is proposed here for computing  
86 robust bifurcation margins. The core idea is to build an LFT model of the Jacobian  
87 of the uncertain vector field (which will generically depend on the states of the system  
88 and on the uncertainties) and to formulate the computation of the closest Hopf bi-  
89 furcation as the worst-case perturbation matrix for which the LFT becomes singular.  
90 This bears similarities to the problem solved by  $\mu$ , but significant differences hold as  
91 commented in the paper. The determination of the margins is posed as a nonlinear  
92 smooth optimization problem, which can be solved with off-the-shelf algorithms. The  
93 program also allows the type of Hopf bifurcation (subcritical or supercritical) to be  
94 specified by constraining the sign of the first Lyapunov coefficient. Since the opti-

mization problem is nonlinear, the issue of local minima is discussed and different strategies are proposed to mitigate it. These include a multi-start strategy based on the construction of a manifold of Hopf points connected to a given solution obtained by the optimizer. The main advantages of the proposed approach, whose formulation is detailed in section 3, include: low dimension and computational cost of the solved problem; improved confidence on the accuracy of the results in terms of global validity of the optimum; possibility to apply the wealth of analysis strategies available with  $\mu$  (e.g., sensitivity analysis, frequency interpretation of the results).

In section 4 the use of this framework to study nonlinear stability problems arising in power system and aerospace applications is investigated by considering two case studies from the literature. First, the sensitivity to a set of physical parameters of the Hopf bifurcation encountered in a power load system with voltage regulator and dynamic load model is considered in section 4.1. It is shown that the application of the robust bifurcation margin allows on one hand to retrieve the same findings reported in [13] (which considered a first-order approximation of the sensitivity), and on the other to investigate more sophisticated types of sensitivity analyses where coupling among uncertain parameters are also accounted for.

Then, an aeroelastic flutter case study is analyzed in section 4.2. Flutter is a self-excited instability in which aerodynamic forces on a flexible body couple with its natural vibration modes producing oscillatory motion. In the presence of nonlinearities, the system typically exhibits loss of stability of the equilibrium in the form of a Hopf bifurcation with ensuing Limit Cycle Oscillations (LCO). Results show a good match with prior studies that considered linear robust analyses [25], and highlight the unique capability of this framework to allow the type of Hopf bifurcation (subcritical or supercritical) of which robustness is studied to be chosen in the analysis.

Bifurcation analysis has been extensively applied to both application fields [41, 11], but the effect of uncertainties has received far less attention. The results in section 4 show that the proposed framework can be a valuable tool for analyzing robustness in the nonlinear context and a more in depth application to these challenging problems is a future research direction.

Preliminary results of this work were presented in [24].

**Notation:**  $[x; y]$  denotes vertical concatenation of two vectors  $x \in \mathbb{R}^n$  and  $y \in \mathbb{R}^m$ .  $|\mathbb{I}|$  indicates cardinality of a set  $\mathbb{I}$ ,  $\bar{\sigma}(P)$  is the maximum singular value of a matrix  $P \in \mathbb{R}^{n \times n}$ ,  $\bar{r}$  is the complex conjugate of  $r \in \mathbb{C}^n$  and  $\langle r, q \rangle = \bar{r}^T q$  is the scalar product between complex vectors  $r, q \in \mathbb{C}^n$ . Where evident from the context, subscripts of vectors and matrices are used to specify their elements (e.g.,  $x_3$  is the third element of  $x \in \mathbb{R}^n$ ); the symbol  $\hat{\cdot}$  is used for solutions of an optimization; the symbol  $\tilde{\cdot}$  is used for uncertain quantities;  $\text{diag}(\cdot)$  indicates a block diagonal matrix made up of elements in  $\cdot$ .

**2. Background.** This section provides an overview on the techniques and tools employed in the work. The first subsection presents the theoretical background of bifurcation (2.1.1) and numerical continuation (2.1.2). This is followed by a short introduction to the robust control concepts of LFT models (2.2.1) and  $\mu$  analysis (2.2.2).

### 2.1. Nonlinear dynamics approaches.

**2.1.1. Bifurcation theory.** Consider an autonomous nonlinear system of the form

$$(2.1) \quad \dot{x} = f(x, p),$$

143 where  $x \in \mathbb{R}^{n_x}$  and  $p \in \mathbb{R}^{n_p}$  are respectively the vectors of states and bifurcation  
 144 parameters, and  $f : \mathbb{R}^{n_x} \times \mathbb{R}^{n_p} \rightarrow \mathbb{R}^{n_x}$  is the vector field. In this work  $f$  is assumed  
 145 to gather smooth nonlinear functions ( $f \in \mathcal{C}^\infty$ ). Therefore, the Jacobian matrix of  
 146 the vector field  $\nabla_x f : \mathbb{R}^{n_x} \times \mathbb{R}^{n_p} \rightarrow \mathbb{R}^{n_x \times n_x}$ , denoted here by  $J$ , is always defined.

147 The vector  $x_0$  is called a fixed point or equilibrium of (2.1) corresponding to  $p_0$   
 148 if  $f(x_0, p_0) = 0$ . Let us denote with  $n_0$  the number of eigenvalues of  $J(x_0, p_0)$  with  
 149 zero real parts, respectively. Then  $x_0$  is called a hyperbolic fixed point if  $n_0 = 0$ ,  
 150 otherwise it is called nonhyperbolic. Bifurcations of fixed points are concerned with  
 151 the loss of hyperbolicity of the equilibrium as  $p$  is varied. Two scenarios can take  
 152 place: static bifurcations and dynamic bifurcations [27, 21]. The former arise when  
 153  $J$  is singular at an equilibrium, i.e., it has a zero eigenvalue. The common feature  
 154 of static bifurcations is that branches of fixed points meet at the bifurcation point.  
 155 In the case of dynamic bifurcations, branches of fixed points and periodic solutions  
 156 meet. This case, also referred to as Hopf bifurcation, is the focus of this work and is  
 157 formally described by the following theorem.

158 **THEOREM 2.1** ([21] Hopf bifurcation theorem). *Suppose that the system  $\dot{x} =$*   
 159  *$f(x, p)$ ,  $x \in \mathbb{R}^{n_x}$  and  $p \in \mathbb{R}$  has an equilibrium  $(x_H, p_H)$  at which the following*  
 160 *properties are satisfied.*

- 161 1.  *$J(x_H, p_H)$  has a simple pair of pure imaginary eigenvalues and no other ei-*  
 162 *genvalues with zero real parts. This implies, for the implicit function theorem,*  
 163 *that there is a smooth curve of equilibria  $(x(p), p)$  with  $x(p_H) = x_H$ . The ei-*  
 164 *genvalues  $\nu(p)$ ,  $\bar{\nu}(p)$  of  $J(x(p))$ , with  $\nu(p_H) = i\omega_H$ , vary smoothly with  $p$ .*
- 165 2. *It holds*

$$166 \quad (2.2) \quad \frac{d}{dp} (\operatorname{Re} \nu(p))|_{p=p_H} = l_0 \neq 0.$$

167 *Then there is a unique three-dimensional center manifold passing through  $(x_H, p_H)$  in*  
 168  *$\mathbb{R}^{n_x} \times \mathbb{R}$  and a smooth system of coordinates for which the Taylor expansion of degree*  
 169 *3 on the center manifold is given in polar coordinates  $(\rho, \theta)$  by*

$$170 \quad (2.3) \quad \begin{aligned} \dot{\rho} &= (l_0 p + l_1 \rho^2) \rho, \\ \dot{\theta} &= \omega + l_2 p + l_3 \rho^2, \end{aligned}$$

171 *where  $l_0, l_1, l_2$ , and  $l_3$  are real coefficients defining the manifold. If  $l_1 \neq 0$ , there is a*  
 172 *surface of periodic solutions in the center manifold which has quadratic tangency with*  
 173 *the eigenspace of  $\nu(p)$ ,  $\bar{\nu}(p)$ . If  $l_1 < 0$ , then these periodic solutions are stable limit*  
 174 *cycles, while if  $l_1 > 0$ , the periodic solutions are repelling.*

175 Note first that the theorem is typically stated considering a scalar  $p$  since the Hopf  
 176 bifurcation is codimension-1. Condition 1 of Th. 2.1 requires that the Jacobian of the  
 177 vector field has a pair of purely imaginary eigenvalues (and no other eigenvalues on the  
 178 imaginary axis). Condition 2, also known as the transversality condition, prescribes  
 179 that these eigenvalues are not stationary with respect to  $p$  at the bifurcation. A  
 180 fundamental parameter determining the dynamic behaviour in the neighborhood of a  
 181 Hopf point is  $l_1$ , also called the first Lyapunov coefficient. Its value determines whether  
 182 the Hopf bifurcation is *subcritical* or *supercritical*, and its analytical expression is given  
 183 by [27]

$$184 \quad (2.4) \quad l_1 = \frac{1}{2\omega_H} \operatorname{Re} \langle r, C(q, q, \bar{q}) - 2B(q, A^{-1}B(q, \bar{q})) + B(\bar{q}, (2i\omega_H I_n - A)^{-1}B(q, q)) \rangle.$$

185 Here the complex vectors  $r, q \in \mathbb{C}^{n_x}$  satisfy

$$186 \quad (2.5) \quad Jq = i\omega_H q, \quad J^T r = -i\omega_H r, \quad \langle r, q \rangle = 1.$$

187 The functions  $B : \mathbb{R}^{n_x} \times \mathbb{R}^{n_x} \rightarrow \mathbb{R}^{n_x}$  and  $C : \mathbb{R}^{n_x} \times \mathbb{R}^{n_x} \times \mathbb{R}^{n_x} \rightarrow \mathbb{R}^{n_x}$  are the tensors  
 188 of second and third order derivatives evaluated at  $x_H$ , respectively. For example, for  
 189 vectors  $\xi, \varsigma, \chi \in \mathbb{R}^{n_x}$ ,  $B(\xi, \varsigma)$  and  $C(\xi, \varsigma, \chi)$  are in  $\mathbb{R}^{n_x}$  with components

$$190 \quad (2.6) \quad B_i(\xi, \varsigma) = \sum_{j,k=1}^{n_x} \frac{\partial^2 f_i(x, p)}{\partial x_j \partial x_k} \Big|_{x=x_H, p=p_H} \xi_j \varsigma_k, \quad i = 1, 2, \dots, n_x,$$

$$C_i(\xi, \varsigma, \chi) = \sum_{j,k,l=1}^{n_x} \frac{\partial^3 f_i(x, p)}{\partial x_j \partial x_k \partial x_l} \Big|_{x=x_H, p=p_H} \xi_j \varsigma_k \chi_l, \quad i = 1, 2, \dots, n_x.$$

191 **2.1.2. Numerical continuation.** The computational tool of bifurcation analy-  
 192 sis is numerical continuation, providing path following algorithms allowing implicitly  
 193 defined manifolds [19] to be computed. These schemes are based on the implicit func-  
 194 tion theorem (IFT) [45], which guarantees, under the condition that  $J$  is non-singular  
 195 at an initial point  $(x_0, p_0)$ , that there exist neighbourhoods  $X$  of  $x_0$  and  $P$  of  $p_0$  and  
 196 a function  $g : P \rightarrow X$  such that  $f(x, p) = 0$  has the unique solution  $x = g(p)$  in  $X$ .  
 197 Examples of numerical techniques to compute the implicit manifold  $g$  are Newton-  
 198 Raphson, arclength, and pseudo-arclength continuation [19], efficiently implemented  
 199 in freely available software, e.g., AUTO [14], and COCO [10].

200 A general continuation problem, so called *extended*, can be formulated as follows  
 201 [9, 10]

$$202 \quad (2.7) \quad F(u, \lambda) := \begin{pmatrix} \Phi(u) \\ \Psi(u) \end{pmatrix} - \begin{pmatrix} 0 \\ \lambda \end{pmatrix} = 0,$$

$$\Phi : \mathbb{R}^{n_u} \rightarrow \mathbb{R}^m, \quad \Psi : \mathbb{R}^{n_u} \rightarrow \mathbb{R}^{n_\lambda},$$

203 where  $\Phi$  defines the zero problem in the vector  $u$  of continuation *variables*,  $\Psi$  denotes  
 204 a family of monitor functions and  $\lambda$  is a vector of continuation *parameters*. It is  
 205 straightforward to see that the goal of tracking equilibria of the vector field  $f$  can  
 206 be pursued by solving the zero problem only with  $\Phi = f$ , and  $u = [x; p]$ . However,  
 207 the extended continuation problem in (2.7) allows for a greater variety of problems  
 208 to be solved, as the related concept of *restricted* continuation problem shows. Let  
 209  $\mathbb{I} \subseteq \{1, \dots, n_\lambda\}$  be an index set and  $\bar{\mathbb{I}}$  its complement in  $\{1, \dots, n_\lambda\}$ . Let  $\lambda_{\mathbb{I}} = \{\lambda_i | i \in \mathbb{I}\}$   
 210 and consider the restriction  $F(u, \lambda)|_{\lambda_{\mathbb{I}} = \lambda_{\mathbb{I}}^*}$  satisfying the IFT at some point  $(u^*, \lambda^* =$   
 211  $\Psi(u^*))$ . Then  $F(u, \lambda)|_{\lambda_{\mathbb{I}} = \lambda_{\mathbb{I}}^*}$  defines a continuation problem for a  $d$ -manifold with  
 212  $d = n_u - (m + |\mathbb{I}|)$ .  $\lambda_{\bar{\mathbb{I}}}$  and  $\lambda_{\mathbb{I}}$  are called the set of active and inactive continuation  
 213 parameters respectively, since the former changes during continuation, while the latter  
 214 remain constant. Analogously, equations corresponding to  $\lambda_{\bar{\mathbb{I}}}$  are inactive constraints,  
 215 while equations corresponding to  $\lambda_{\mathbb{I}}$  are active constraints, because they impose an  
 216 additional condition on the solutions to the set of zero problems. The formulation  
 217 (2.7) is implemented in the software COCO, which is used for all the continuation  
 218 analyses performed in this work.

## 219 2.2. Robust control theory.

220 **2.2.1. The Linear Fractional Transformation paradigm.** Linear Fractional  
 221 Transformation (LFT) is an instrumental tool in robust control theory for analysis

222 and control of uncertain systems [48]. For the sake of clarity, first an intuition of the  
 223 reasoning behind LFT is given, followed by a more formal definition.

224 The classic interpretation of an LFT is in terms of input to output relationship of  
 225 a feedback interconnection. Let us consider a linear time invariant (LTI) system with  
 226 transfer matrix (i.e. matrix of transfer functions)  $M_{22} \in \mathbb{C}^{p_2 \times q_2}$ , input  $v$  and output  
 227  $y$ . The system  $M_{22}$  is assumed to be exactly known, and thus is also termed *nominal*.  
 228 If the model has uncertainties (which will be better characterized later), these can be  
 229 modelled with an operator  $\Delta_u \in \mathbb{C}^{q_1 \times p_1}$  with input  $z$  and output  $w$ . The effect of  $\Delta_u$   
 230 on  $M_{22}$  can then be described by introducing the transfer matrices  $M_{11}$ ,  $M_{12}$  and  $M_{21}$ .  
 231 For example, in the case of parametric uncertainties, these will be simply static (gain)  
 232 matrices, while for the case of unmodelled dynamics these could also have dynamic  
 233 terms (e.g. low pass filters). The key point is that, by choosing these matrices, the  
 234 analyst can describe with a certain flexibility how the perturbation affects the nominal  
 system. Given this setting, Figure 1 shows the standard representation of LFT.

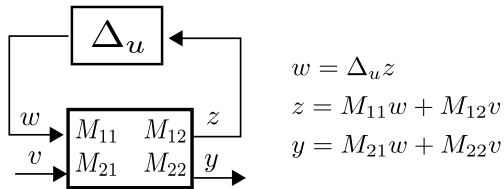


FIG. 1. Standard feedback representation of an LFT.

235

236 The central idea is thus to represent the uncertain system as a feedback of known  
 237 components (the transfer matrices  $M_{ij}$ ) with uncertain (the operator  $\Delta_u$ ) ones. In  
 238 practice, this is done by pulling out of the system the unknown parts, so that the  
 239 problem appears as a nominal system subject to an artificial feedback. Available  
 240 toolboxes [28] allow this operation to be efficiently performed and provide the analyst,  
 241 given a description of how the uncertainties affect the system, with the matrices  $M_{ij}$ .

242 In order to formally define an LFT, let us denote by  $M \in \mathbb{C}^{(p_1+p_2) \times (q_1+q_2)}$  the  
 243 partitioned transfer matrix (also termed *coefficient matrix*)

$$244 \quad (2.8) \quad M = \begin{bmatrix} M_{11} & M_{12} \\ M_{21} & M_{22} \end{bmatrix},$$

245 and let  $\Delta_u \in \mathbb{C}^{q_1 \times p_1}$  the uncertain operator. The LFT of  $M$  with respect to  $\Delta_u$  is  
 246 defined as the map  $\mathcal{F} : \mathbb{C}^{q_1 \times p_1} \rightarrow \mathbb{C}^{p_2 \times q_2}$

$$247 \quad (2.9) \quad \mathcal{F}(M, \Delta_u) = M_{22} + M_{21} \Delta_u (I - M_{11} \Delta_u)^{-1} M_{12}.$$

248 With reference to Fig. 1,  $\mathcal{F}(M, \Delta_u)$  compactly defines the uncertain transfer matrix  
 249 from input  $v$  to output  $y$  of the nominal system  $M_{22}$  when this is subject to  $\Delta_u$ .  
 250 Indeed, for  $\Delta_u = 0$  (no uncertainties in the model) it holds  $\mathcal{F}(M, \Delta_u) = M_{22}$ . It is  
 251 also important to observe that  $M_{11}$  is, within this input to output framework, the  
 252 transfer matrix seen by the perturbation block  $\Delta_u$ . A crucial feature apparent in (2.9)  
 253 is that the LFT is well posed if and only if the inverse of  $(I - M_{11} \Delta_u)$  exists. Otherwise,  
 254  $\mathcal{F}(M, \Delta_u)$  is said to be singular. Singularity of the LFT is typically associated with the  
 255 loss of stability of the underlying uncertain system, and thus finding the uncertain  
 256 perturbations for which this happens is typically the objective of robust stability  
 257 analysis (details on this will be provided in Sec. 2.2.2).

258 In robust control,  $\Delta_u$  typically gathers parametric and dynamic uncertainties and  
 259 can be represented as

$$260 \quad (2.10) \quad \Delta_u = \text{diag}(\delta_i I_{d_i}, \delta_j I_{d_j}, \Delta_{D_k}),$$

$$i = 1, \dots, n_R, \quad j = n_R + 1, \dots, n_R + n_C, \quad k = 1, \dots, n_D,$$

261 where the uncertainties associated with  $n_R$  real scalars  $\delta_i$ ,  $n_C$  complex scalars  $\delta_j$ ,  
 262 and  $n_D$  unstructured (or full) complex blocks  $\Delta_{D_k}$  are listed in diagonal format.  
 263 The identity matrices of dimension  $d_i$  and  $d_j$  take into account the fact that scalar  
 264 uncertainties might be repeated in  $\Delta_u$  when the LFT of the system is built up. For  
 265 example, if a matrix has the parameter  $\delta_i$  on three different rows, in order to cast  
 266 it in the form of an LFT (2.9) it will be necessary to have  $d_i=3$  [28]. Typically the  
 267 uncertain parameters are normalized by scaling of  $M$  such that  $\Delta_u = 0$  coincides with  
 268 the nominal system (i.e., uncertain parameters at their nominal values) and  $\bar{\sigma}(\Delta_u) \leq 1$   
 269 when uncertainties take values in the allowed interval. The set in (2.10) is generally  
 270 referred to as *structured* because of the block diagonal structure. This feature, enabled  
 271 by the LFT modeling paradigm, is known to provide less conservative results in the  
 272 analysis of uncertain systems with respect to unstructured representations (used, for  
 273 example, in the celebrated small gain theorem [48]).

274 This work leverages the LFT framework for analysis of nonlinear systems. The  
 275 interpretation given previously, while providing insights into this paradigm, cannot  
 276 be thus readily used since it requires transfer matrices. For this reason, an alternative  
 277 viewpoint on LFT is proposed.

278 Let us start by considering the state-space (SS) representation  $(\mathcal{A}, \mathcal{B}, \mathcal{C}, \mathcal{D})$  of the  
 279 nominal LTI system with transfer matrix  $M_{22}$

$$280 \quad (2.11a) \quad \begin{cases} \dot{x} = \mathcal{A}x + \mathcal{B}v, \\ y = \mathcal{C}x + \mathcal{D}v, \end{cases}$$

$$281 \quad (2.11b) \quad M_{22}(s) = \mathcal{D} + \mathcal{C}(sI_{n_x} - \mathcal{A})^{-1}\mathcal{B},$$

283 where  $s$  is the Laplace variable. Define now

$$284 \quad (2.12) \quad M_\nu = \begin{bmatrix} \mathcal{A} & \mathcal{B} \\ \mathcal{C} & \mathcal{D} \end{bmatrix}, \quad \Delta_\nu = \frac{1}{s}I_{n_x}.$$

285 It can then be shown that  $\mathcal{F}(M_\nu, \Delta_\nu) = M_{22}$ . This follows directly from

$$286 \quad (2.13) \quad \mathcal{F}(M_\nu, \Delta_\nu) = \mathcal{D} + \mathcal{C} \frac{1}{s}I_{n_x} (I_{n_x} - \frac{1}{s}\mathcal{A})^{-1} \mathcal{B} = \mathcal{D} + \mathcal{C}(sI_{n_x} - \mathcal{A})^{-1} \mathcal{B} = M_{22}(s),$$

287 where the diagonal structure of  $\Delta_\nu$  and the fact that  $\frac{1}{s} \neq 0$  have been exploited.  
 288 This result shows that the LFTs generalize the realization of transfer matrices into  
 289 state-space (SS) representations to the case of rational multivariate matrices. For this  
 290 reason, the LFT paradigm can also be regarded as a realization technique [28].

291 This interpretation also highlights a paramount aspect for the present work. The  
 292 poles of (2.11) are typically found via eigenvalue analysis of  $\mathcal{A}$ . Equivalently, the  
 293 system has a given pole  $\nu$  if  $(\nu I_{n_x} - \mathcal{A})^{-1}$  is singular. Note that this latter condition  
 294 can be formulated as the singularity of the LFT  $\mathcal{F}(M_\nu, \Delta_\nu)$  by replacing  $s = \nu$ . In  
 295 particular, the LTI (2.11) has a purely imaginary eigenvalue (i.e. it is neutrally stable)  
 296 if there exists  $\omega > 0$  for which  $\mathcal{F}(M_\nu, \Delta_\nu)$  is singular with  $s = i\omega$ .

297 Let us consider now the case when the LTI system (2.11) is subject to uncertain-  
 298 ties. The problem can be described with the LFT formalism considering two blocks



299 for the *uncertain* operator, namely  $\Delta_u$  containing the structured perturbations, and  
 300  $\Delta_\nu$ . The coefficient matrix  $M$  is partitioned correspondingly

$$301 \quad (2.14) \quad M = \begin{bmatrix} \mathcal{A} & \mathcal{A}_{12} & \mathcal{B} \\ \mathcal{A}_{21} & \mathcal{A}_{22} & \mathcal{B}_1 \\ \mathcal{C} & \mathcal{C}_1 & \mathcal{D} \end{bmatrix}, \quad \Delta = \text{diag}(\Delta_\nu, \Delta_u).$$

302 A pictorial representation of the LFT  $\mathcal{F}(M, \Delta)$  defined by the operators in (2.14) is  
 303 given in Figure 2.

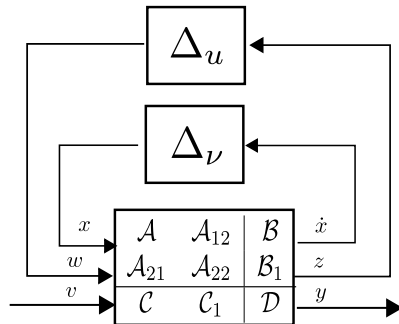


FIG. 2. LFT of an uncertain state-space model.

304 The difference between the representations in Figure 1 and Figure 2, both describ-  
 305 ing an uncertain system, is that in the former the system is described via its transfer  
 306 matrices, while in the latter a state-space representation is used. One can switch from  
 307 the first to the second representation by exploiting the fact that  $\mathcal{F}(M_\nu, \Delta_\nu) = M_{22}$   
 308 (which was proved above).

309 The consequence of this change of representation is that the new block  $\Delta_\nu$  appears.  
 310 Correspondingly, the coefficient matrix  $M$  (2.14) now features the matrix  $M_\nu$  (2.12)  
 311 plus other matrices describing the effect of the uncertainties on the state-matrices.  
 312 Note indeed that the transfer matrices  $M_{11}$ ,  $M_{12}$  and  $M_{21}$  will also be expressed here  
 313 with their SS representation. Let us assume now that (2.11) is nominally stable (i.e.  
 314  $\mathcal{A}$  has all the eigenvalues in the left half-plane). Then the uncertain LTI system has  
 315 a purely imaginary eigenvalue if there exist  $\omega > 0$  (with  $s = i\omega$ ) and a combination  
 316 of the uncertainties in  $\Delta_u$  for which  $\mathcal{F}(M, \Delta)$  (2.14) is singular.

317 The advantage of this representation, which is key for the present work, is that  
 318 LFTs can be constructed even for systems which do not have transfer matrices, if an  
 319 *appropriate* state-space description is available. Sec. 3.1 will be devoted to showing  
 320 which crucial steps can be taken in order to apply this rationale to the prototype of  
 321 vector field introduced in (2.1).

322 Note finally that a useful property when dealing with LFTs featured by distinct  
 323  $\Delta$ -blocks is that interconnections of LFTs can be rewritten as one single LFT. This  
 324 is only a numerical aspect relative to the construction of LFT models, but it greatly  
 325 helps to separate modeling-specific details of the system under consideration and to  
 326 ease the algebraic manipulations. By virtue of this, it holds for the LFT defined in  
 327 (2.14)

$$328 \quad (2.15) \quad \mathcal{F}(M, \Delta) = \mathcal{F}(\mathcal{F}(M, \Delta_\nu), \Delta_u).$$

329 **2.2.2.  $\mu$  analysis.** The  $\mu$  analysis technique leverages the key features of LFT  
 330 modeling reviewed in the previous section to address the robust stability analysis of

331 LTI systems in the face of uncertainties. The structured singular value is a matrix  
 332 function denoted by  $\mu_{\Delta}(M)$  and several equivalent definitions are available in the  
 333 literature [48, 15, 35]. A definition which encompasses the aspects relevant to this  
 334 work is

$$335 \quad (2.16) \quad \mu_{\Delta}(M) = \left( \min_{\Delta} (\kappa : \mathcal{F}(\mathcal{F}(M, \Delta_{\nu}), \Delta_u) \text{ is singular, } \bar{\sigma}(\Delta_u) \leq \kappa) \right)^{-1},$$

336 where  $\kappa$  is a real positive scalar, and  $\mu_{\Delta}(M) = 0$  if the minimization problem has no  
 337 solution.

338 Based on the point of view of LFT as realization technique, an interpretation of  
 339 the  $\mu$  analysis technique is as *worst-case* eigenvalue analysis for uncertain systems.  
 340 Let us focus on the operator  $\Delta$  of the LFT  $\mathcal{F}(M, \Delta)$  defined in (2.14). The block  
 341  $\Delta_{\nu}$  does not represent a true uncertainty of the system, and its meaning is that the  
 342 singularity of the LFT is checked against all the possible eigenvalues on the imaginary  
 343 axis. For the sake of understanding, one can think of realizing this block by considering  
 344 a set of frequencies  $\omega$  and evaluating  $\Delta_{\nu}$  at  $\nu = i\omega$ . By doing this,  $\Delta = \Delta_u$  and the  
 345 problem defined in (2.16) consists of finding the perturbation matrix with the smallest  
 346 maximum singular value (also termed worst-case matrix) such that the uncertain  
 347 system has a pair of purely imaginary eigenvalues  $\pm i\omega$ . Therefore,  $\mu_{\Delta}(M)$  provides a  
 348 robust stability (RS) test for an uncertain linear system. Specifically, if  $\mu_{\Delta}(M) \geq 1$  a  
 349 candidate (i.e., within the allowed range of the uncertainty set) perturbation matrix  
 350 exists that violates the well-posedness of  $\mathcal{F}(M, \Delta)$ . In essence, the uncertain state-  
 351 matrix has the eigenvalues  $s = \pm i\omega$  for a certain combination of the uncertainties  
 352 in the allowed range. On the contrary, if  $\mu_{\Delta}(M) < 1$  then there is no perturbation  
 353 matrix inside the set  $\Delta$  such that the  $\mathcal{F}(M, \Delta)$  is ill-posed and thus the system is  
 354 robust stable within the range of uncertainties considered.

355 In the most established algorithms [2],  $\mu$  is evaluated on a discretized frequency  
 356 range. That is, the  $\Delta_{\nu}$  block is realized as discussed before on a pre-selected grid  
 357 of frequencies, and the corresponding set of matrices  $M(i\omega)$  (the dependence on the  
 358 frequency is now stressed) is computed. Subsequently,  $\mu_{\Delta}(M(i\omega))$  is computed and  
 359 a frequency-domain representation of the results is obtained. This is done in order  
 360 to avoid the need to solve the optimization problem (2.16) on a continuous range of  
 361 frequency, which proves computationally challenging. An exception to this common  
 362 practice worth mentioning is represented by recently developed Hamiltonian-based  
 363 algorithms (i.e. SMART library [39] and Robust Control Toolbox from MATLAB  
 364 R2016b) which guarantees the validity of results over a continuous range of frequen-  
 365 cies.

366 Finally, note that (2.16) is an NP-hard problem with either pure real or mixed  
 367 real-complex uncertainties [5], thus all  $\mu$  algorithms work by searching for upper  
 368 and lower bounds. The upper bound  $\mu_{UB}$  provides the maximum size perturbation  
 369  $\bar{\sigma}(\Delta_u^{UB}) = 1/\mu_{UB}$  for which RS is guaranteed, whereas the lower bound  $\mu_{LB}$  defines  
 370 a minimum size perturbation  $\bar{\sigma}(\Delta_u^{LB}) = 1/\mu_{LB}$  for which RS is guaranteed to be  
 371 violated. Along with this information, the lower bound also provides the matrix  $\Delta_u^{LB}$   
 372 determining singularity of the LFT.

373 **3. Main results.** In this section the main result of the work is presented. The  
 374 problem addressed by this article is formally defined in section 3.1 and in section  
 375 3.2 a solution by means of a nonlinear optimization program is proposed. The step-  
 376 by-step presentation, from Program 3.1, which calculates the *smallest* perturbations  
 377 making the Jacobian unstable, to Program 3.4, which computes the closest subcritical

378 and supercritical Hopf bifurcations, aims at clearly presenting the formulation of  
 379 robust bifurcation margins. Note that only [Program 3.2](#) and [Program 3.4](#) are actually  
 380 needed to solve the problem (depending on whether the type of Hopf bifurcation is  
 381 specified or not). In section [3.3](#) a multi-start strategy is described, within the extended  
 382 continuation paradigm, to mitigate the issue of local optima. Finally, in section [3.4](#) a  
 383 critical comparison with an alternative method from the literature solving a similar  
 384 problem is discussed.

385 **3.1. Problem statement.** The usual starting point in bifurcation analysis is  
 386 Eq. [\(2.1\)](#), where  $f$  is a *nominal* vector field, meaning that the only dependence  
 387 is on the state  $x$  and bifurcation parameter  $p$ . The latter is of size  $n_p = 1$  for  
 388 continuation of equilibrium points since all their bifurcations have codimension 1, and  
 389 thus 1 parameter is sufficient for its analysis (this of course includes the case of Hopf  
 390 bifurcations, see [Theorem 2.1](#)). Consider the case when parametric uncertainties affect  
 391 the dynamics, e.g. because of lack of confidence on the values of model parameters or  
 392 simplifying assumptions underlying the model. The presence of uncertainties can be  
 393 modelled by introducing the uncertainty vector  $\delta$

$$394 \quad (3.1) \quad \delta = [\delta_1; \dots; \delta_i; \dots; \delta_{n_\delta}], \quad \delta \in \mathbb{R}^{n_\delta}.$$

395 The vector field depends now on  $\delta$ , in addition to  $x$  and  $p$ . To highlight this, we  
 396 denote the uncertain vector field by  $\tilde{f}$  and the associated Jacobian by  $\tilde{J}$

$$397 \quad (3.2a) \quad \dot{x} = \tilde{f}(x, p, \delta),$$

$$398 \quad (3.2b) \quad \tilde{f} : \mathbb{R}^{n_x} \times \mathbb{R} \times \mathbb{R}^{n_\delta} \rightarrow \mathbb{R}^{n_x}, \quad \tilde{f} \in \mathcal{C}^\infty,$$

$$399 \quad (3.2c) \quad \tilde{J} : \mathbb{R}^{n_x} \times \mathbb{R} \times \mathbb{R}^{n_\delta} \rightarrow \mathbb{R}^{n_x \times n_x}.$$

401 The objective of the work is then to compute the margins of stable equilibria from the  
 402 closest Hopf bifurcation for nonlinear systems affected by parametric uncertainties.  
 403 To better understand this, assume that the nominal system  $f$  has a Hopf bifurcation  
 404 point  $(x_H, p_H)$ , while for another value of the bifurcation parameter  $\bar{p}_0$  a stable fixed  
 405 point  $\bar{x}_0$  exists for  $f$ . The goal is to determine the *smallest* (or *worst-case*) perturba-  
 406 tion  $\bar{\delta} \in \delta$  such that  $\tilde{f}$  undergoes a Hopf bifurcation at  $\bar{p}_0$ . It is key to observe that the  
 407 Hopf bifurcation is triggered by perturbations in  $\delta$ , while the bifurcation parameter  
 408 is fixed at  $\bar{p}_0$ . The reason for this is that the aim here is to compute the *margin* of  
 409 a certain condition from the occurrence of the bifurcation. Thus,  $p$ , which generally  
 410 defines an operating condition (e.g. load power in an electric power system, speed for  
 411 an aircraft) is kept fixed at the value  $\bar{p}_0$  which identifies the condition for which the  
 412 margin is computed. This is different from what is done in the direct method [\[12\]](#)  
 413 (the other approach that looked at a similar problem) where there is no distinction  
 414 between bifurcation and uncertain parameters, both collected in  $p$  (which is then mul-  
 415 tidimensional). As a result of this, all the entries of  $p$  are allowed to be perturbed in  
 416 order to trigger the bifurcation, whereas here the distinction between  $p$  (of dimension  
 417 1) and  $\delta$  (of dimension  $n_\delta$ , depending on how many uncertainties are considered) is  
 418 clear. See section [3.4](#) for a thorough comparison with the direct method.

419 It is often relevant to distinguish between supercritical and subcritical Hopf bifurca-  
 420 tions, hence two distinct worst-case perturbations will be considered. For the sake  
 421 of readability, this distinction will be highlighted in the text when relevant but the  
 422 notation used will be  $\bar{\delta}$  in both cases.

423 In order to quantify the margin to the closest bifurcation, and thus to allow the  
 424 concept of worst-case uncertainty to be formalized, a metric for the magnitude of the

425 perturbation must be adopted. The adopted metric should measure in some quanti-  
 426 tative form the perturbation to which the system is subject. This task is arbitrary  
 427 and a common approach from robust control is followed [48] (see also section 2.2.2).

428 Consider a generic uncertain parameter  $d$ , with  $w_d$  indicating the uncertainty level  
 429 with respect to a nominal value  $d_0$  and  $\delta_d \in [-1, 1]$  representing the normalized un-  
 430 certainty range. Note that  $d_0$  and  $w_d$  are typically fixed by the analyst based on the  
 431 knowledge of the nominal value and dispersion of the parameter  $d$  respectively. A  
 432 multiplicative uncertain representation of  $d$  is thus obtained as

$$433 \quad (3.3) \quad d = (1 + w_d \delta_d) d_0,$$

434 where  $\delta_d = 0$  corresponds to the nominal value of  $d$ , while  $\delta_d = \pm 1$  represents a  
 435 perturbation at the extreme of the parameter range (e.g., a variation of  $\pm 20\%$  from  $d_0$   
 436 if  $w_d = 0.2$ ). Once the normalization (3.3) is applied to all the uncertain parameters in  
 437 (3.1), a possible scalar metric (or norm) to quantify the magnitude of the perturbation  
 438 is the largest of the absolute values of the elements in  $\delta$ . This can be equivalently  
 439 expressed as  $\bar{\sigma}(\text{diag}(\delta))$ , i.e., the maximum singular value of the diagonal matrix with  
 440 elements of  $\delta$  on the diagonal. Such a metric quantifies the deviation of the uncertain  
 441 parameters from their nominal values along the direction of the parameter space  
 442 where this is largest. The objective is thus to compute the perturbation vector with  
 443 the smallest possible norm, providing therefore the distance from the closest Hopf  
 444 bifurcation.

445 In fact,  $k_m = \bar{\sigma}(\text{diag}(\delta))$  can be regarded as a robust margin from bifurcation be-  
 446 cause  $k_m \leq 1$  means that a candidate (i.e., within the allowed range of the uncertainty  
 447 set) perturbation exists which determines a Hopf bifurcation. Thus, the equilibrium  
 448  $\bar{x}_0$  of the nominal vector field is not robustly stable at  $\bar{p}_0$ . On the contrary, if  $k_m > 1$   
 449 then there is no perturbation inside the allowed set which is capable of prompting a  
 450 Hopf bifurcation. This is pictorially represented in Figure 3, where on the x-axis is  
 451 reported the bifurcation parameter and on the y-axis the margin  $k_m$  (note that the  
 452 case  $\bar{p}_0 < p_H$  where a Hopf bifurcation is encountered by increasing  $p$  is assumed here  
 453 without loss of generality). When the line  $k_m = 1$  is crossed, the system is operated in  
 454 a region where Hopf bifurcations can occur in the face of the uncertainties accounted  
 for in the system (shaded area).

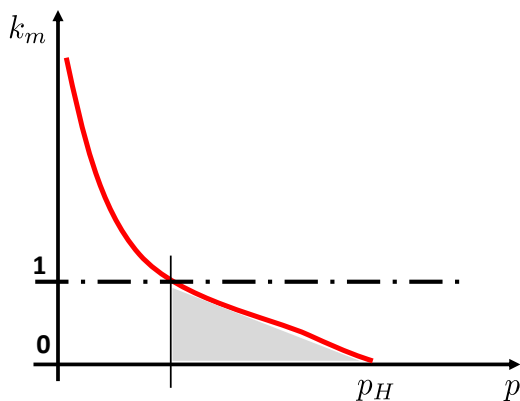


FIG. 3. Concept of robust bifurcation margins.

456 **3.2. Solution via nonlinear optimization.** The fundamental idea to address  
 457 the stated objective is to exploit the interpretation of LFTs discussed in Sec. 2.2.1.  
 458 Consider for a moment only Condition 1 of [Theorem 2.1](#), which prescribes a pair of  
 459 purely imaginary eigenvalues for the Jacobian. If  $\tilde{J}$  is interpreted as the uncertain  
 460 state-matrix of the linear case, an LFT model of the former with respect to the  
 461 uncertain parameters in  $\delta$  can be built up (numerically or analytically [29]). The  
 462 main difference from the linear case is that in general  $\tilde{J}$  is also a function of the states  
 463 of the system  $x$ . This reflects the fact that in the nonlinear context uncertainties  
 464 have a twofold effect on stability. They directly affect the matrix  $\tilde{J}$  as independent  
 465 variables, but also indirectly by changing the location of the equilibrium (around  
 466 which the vector field is linearized). The latter is a distinctive feature of the nonlinear  
 467 setting, since in the linear case the location of the equilibrium does not have any effect  
 468 on the spectrum of the state-matrix, and thus on stability. In full generality, the LFT  
 469 of the Jacobian  $\mathcal{F}(M_{\tilde{J}}, \Delta)$  can be written as

$$470 \quad (3.4a) \quad \mathcal{F}(M_{\tilde{J}}, \Delta) = \mathcal{F}(\mathcal{F}(\mathcal{F}(M_{\tilde{J}}, \Delta_\nu), \Delta_x), \Delta_u),$$

$$471 \quad (3.4b) \quad \Delta = \text{diag}(\Delta_u, \Delta_x, \Delta_\nu), \quad M_{\tilde{J}} = [M_{\tilde{J}_{11}} M_{\tilde{J}_{12}}; M_{\tilde{J}_{21}} M_{\tilde{J}_{22}}],$$

$$472 \quad (3.4c) \quad \Delta_u = \text{diag}(\delta_1 I_{d_1}, \dots, \delta_i I_{d_i}, \dots, \delta_{n_\delta} I_{d_{n_\delta}}),$$

$$473 \quad (3.4d) \quad \Delta_x = \text{diag}(x_1 I_{x_1}, \dots, x_j I_{x_j}, \dots, x_{n_x} I_{x_{n_x}}),$$

$$474 \quad (3.4e) \quad \Delta_\nu = \frac{1}{\nu} I_{n_x}, \quad \nu = i\omega,$$

476 where (3.4a) exploits the property of interconnected LFTs, and  $\Delta_u$  is a particular  
 477 instance of the structured uncertainty set defined in (2.10), considering only real pa-  
 478 rameters. Compared to the linear case (2.15),  $\Delta$  features now an additional structured  
 479 block  $\Delta_x$ , which arises when performing the LFT modeling of  $\tilde{J}$  due to the states ex-  
 480 plicitly appearing in the Jacobian, and for which a similar representation to the one  
 481 for  $\Delta_u$  is employed.  $\Delta_\nu$  finally restricts the attention to purely imaginary eigenvalues  
 482 of  $\tilde{J}$  with frequency  $\omega$ .

483 Condition 1 of [Theorem 2.1](#) can then be expressed as the singularity of the LFT  
 484 (3.4a). This is the central step of the proposed extension of  $\mu$  from the linear con-  
 485 text, where  $\tilde{J}$  would be the uncertain state-matrix, to the nonlinear one. In fact,  $\mu$   
 486 computes by definition the worst-case perturbation matrix which makes the underly-  
 487 ing LFT ill-posed and employs the same metric (2.16) as the one used to define the  
 488 robust bifurcation margin  $k_m$ . It follows indeed from the definitions and properties  
 489 commented earlier that  $k_m = \bar{\sigma}(\text{diag}(\delta)) = \bar{\sigma}(\Delta_u)$ . Specifically,  $k_m$  is the reciprocal  
 490 of  $\mu$  and it has been adopted here because of its straightforward meaning of distance  
 491 (or margin) to the onset of a bifurcation. Note in this regard that the symbol  $k_m$   
 492 was used in the early stages of robust control with the name of *excess stability margin*  
 493 [43, 42].

494 The discussion above paves the way for the nonlinear program presented next,  
 495 which aims to compute the smallest perturbation for which  $\tilde{J}$  has a pair of purely  
 496 imaginary eigenvalues.

PROGRAM 3.1.

$$\begin{aligned} (3.5a) & \\ (3.5b) & \min_X k_m \quad \text{such that} \\ (3.5c) & \end{aligned} \left\{ \begin{array}{l} \tilde{f}(x, \bar{p}_0, \delta) = 0, \\ \mathcal{F}(M_{\tilde{J}}, \Delta) \text{ is singular,} \\ \bar{\sigma}(\Delta_u) \leq k_m, \end{array} \right.$$

497

498

$$X = [x; \delta; \omega],$$

499 where  $X$  is the vector of optimization variables including: states  $x$ ; uncertain param-  
 500 eters  $\delta$ ; and frequency  $\omega$ .  $\tilde{X}$  will indicate the solution vector gathering  $\hat{x}$ ,  $\hat{\delta}$ , and  $\hat{\omega}$   
 501 respectively. Let us examine the constraints of the program. Eq. (3.5a) guarantees  
 502 that the solution  $(\hat{x}, \hat{\delta})$  corresponds to an equilibrium point for the system. Eq. (3.5b)  
 503 ensures that  $\tilde{J}$  has a pair of complex eigenvalues  $\nu = \pm\hat{\omega}$ , and Eq. (3.5c) bounds the  
 504 size of the perturbation matrix.

505 This is a similar optimization problem to that in (2.16), with two crucial dif-  
 506 ferences: constraint (3.5a), and the addition of  $\Delta_x$  in the block  $\Delta$  of  $\mathcal{F}(M_{\tilde{J}}, \Delta)$  (to  
 507 which, notably, constraint (3.5c) does not apply). Due to these differences, available  
 508 algorithms for  $\mu$  cannot be applied to compute solutions of (3.5), thus alternative ways  
 509 should be pursued. Let us examine closely (3.5b), which prescribes singularity of an  
 510 LFT. According to the definition given in (2.9), necessary and sufficient condition  
 511 for the well-posedness of a generic LFT  $\mathcal{F}(M, \Delta_u)$  is the existence of the inverse of  
 512 the matrix  $(I - M_{11}\Delta_u)$ . Note that  $M_{11}$  is, as also previously observed, the transfer  
 513 matrix seen by the perturbation block  $\Delta_u$ . In the context of the LFT  $\mathcal{F}(M_{\tilde{J}}, \Delta)$   
 514 introduced in (3.4), this means that the singularity constraint (3.5b) holds if and only  
 515 if  $\det(I - M_{\tilde{J}11}\Delta) = 0$ . This, in turn, can be recast as nonlinear constraints in the  
 516 optimization variables  $X$ .

517 As for (3.5c), this is a non-smooth constraint because of the maximum singular value  
 518 operator, but it can be drastically simplified by exploiting the structure of  $\Delta_u$  (3.4c).  
 519 Indeed this constraint is equivalent to

$$520 \quad (3.6) \quad -k_m \leq \delta_i \leq k_m, \quad i = 1, \dots, n_\delta,$$

521 which is a set of linear inequalities in the optimization variables and the objective  
 522 function  $k_m$ . Note that a similar relaxation would hold also for complex scalar uncer-  
 523 tainties, not considered in this work.

524 Based on the previous discussion, the following smooth nonlinear optimization  
 525 problem is proposed to solve Program 3.1.

PROGRAM 3.2.

$$\begin{aligned} (3.7a) & \quad \tilde{f}(x, \bar{p}_0, \delta) = 0, \\ (3.7b) & \quad \min_X k_m \quad \text{such that} \quad \det(I - M_{\tilde{J}11}\Delta) = 0, \\ (3.7c) & \quad -k_m \leq \delta_i \leq k_m, \quad i = 1, \dots, n_\delta, \end{aligned}$$

526

$$527 \quad X = [x; \delta; \omega], \quad n_{ctrs} = n_x + 2 + n_\delta,$$

528 where  $n_{ctrs}$  denotes the number of total constraints of the optimization.

529 The key idea behind Program 3.2 is to enforce singularity of the LFT (3.5b) by  
 530 using directly the determinant condition represented by constraint (3.7b). In [40]  
 531 this is listed among the known methods for the computation of  $\mu_{LB}$ , and examples  
 532 of related algorithms can be found in [22, 47]. The approaches presented in those  
 533 works, however, are limited to the case of linear systems, i.e., they represent alter-  
 534 natives to well-established  $\mu$  lower bounds algorithms such as the power iteration  
 535 [36] and the gain-based method [44]. To the best of the authors' knowledge, this  
 536 is indeed the first time that the concept of structured singular value is used in the  
 537 context of worst-case bifurcations of a nonlinear vector field. Moreover, Program 3.2  
 538 recasts the optimization so that the objective function and the constraints are smooth.  
 539 This differs from the aforementioned works where the optimization was performed by  
 540 minimizing the nonsmooth function  $\bar{\sigma}(\Delta_u)$ . This is overcome here by considering

541 the relaxation commented in (3.6) and introducing the objective function  $k_m$  as an  
542 additional optimization variable.

543 *Remark 3.1.* Constraint (3.7b) consists of two (real and imaginary parts of the  
544 determinant) nonlinear equality constraints in the variables  $X$ . By using Laplace  
545 expansion of the determinant [1] and the fact that  $\Delta$  is structured, an analytical  
546 expression for the gradient of (3.7b) with respect to  $\delta$  and  $x$  can be obtained and  
547 provided to the optimizer. As for  $\omega$ , this is more tedious and therefore finite differences  
548 are employed.

549 Note also that, from a continuation perspective, (3.7b) can be regarded as an analog  
550 of the real scalar test functions commonly used to detect Hopf bifurcations [3]. The  
551 latter can be efficiently formulated by means of bordered matrices techniques and  
552 have the property that the test function has a zero at a bifurcation point. The main  
553 difference here is that (3.7b) is complex, thus consists of two real scalar equations.  
554 This is due to the fact that the frequency  $\omega$  of the purely imaginary eigenvalues appear  
555 explicitly in the constraint (and thus is an additional independent variable), which  
556 is different from the test functions formulation. This is an important feature of the  
557 developed approach, and possible ways to exploit it will be discussed later.

### 558 Enforcing the transversality condition

559 *Program 3.2* allows worst-case perturbations to be computed such that the Ja-  
560 cobian of  $\tilde{f}$  linearized around the perturbed equilibrium point has a pair of purely  
561 imaginary eigenvalues. This, however, does not guarantee that the perturbed system  
562 undergoes a Hopf bifurcation because transversality (Condition 2 of Theorem 2.1) is  
563 not automatically verified. Constraints guaranteeing that transversality is satisfied  
564 can be appended to (3.7) in different ways, including using test functions [3] or au-  
565 tomatic differentiation [23]. Here an approach leveraging the versatility of the LFT  
566 paradigm is proposed. Consider a small fixed constant  $\epsilon_p$  which defines the perturbed  
567 bifurcation parameter  $\bar{p}_{\epsilon_p} = (1 + \epsilon_p)\bar{p}_0$ . The LFT  $\mathcal{F}(M_J^\epsilon, \Delta^\epsilon)$  of the Jacobian at  $\bar{p}_{\epsilon_p}$   
568 can be written following (3.4) as

$$569 \quad (3.8a) \quad \mathcal{F}(M_J^\epsilon, \Delta^\epsilon) = \mathcal{F}(\mathcal{F}(\mathcal{F}(M_J^\epsilon, \Delta_\nu^\epsilon), \Delta_x^\epsilon), \Delta_u),$$

$$570 \quad (3.8b) \quad \Delta^\epsilon = \text{diag}(\Delta_u, \Delta_x^\epsilon, \Delta_\nu^\epsilon), \quad M_J^\epsilon = \begin{bmatrix} M_{J_{11}}^\epsilon & M_{J_{12}}^\epsilon & & \\ & M_{J_{21}}^\epsilon & M_{J_{22}}^\epsilon & \\ & & & \end{bmatrix},$$

$$571 \quad (3.8c) \quad \Delta_x^\epsilon = \text{diag}((1 + \epsilon_x)x_1 I_{x_1}, \dots, (1 + \epsilon_x)x_j I_{x_j}, \dots, (1 + \epsilon_x)x_{n_x} I_{k_{n_x}}),$$

$$572 \quad (3.8d) \quad \Delta_\nu^\epsilon = \frac{1}{\nu^\epsilon} I_{n_x}, \quad \nu^\epsilon = \epsilon_\nu + (1 + \epsilon_\omega)\omega,$$

574 where  $\epsilon_\nu$ ,  $\epsilon_x$ , and  $\epsilon_\omega$  are unknown scalars described later. The following optimization  
575 problem is then proposed to determine the worst-case perturbation for which both  
576 conditions of the Hopf theorem are guaranteed to hold, that is, to calculate the margins  
577 to the closest Hopf bifurcation point.

### PROGRAM 3.3.

$$\begin{aligned} (3.9a) & \\ (3.9b) & \\ (3.9c) & \min_X k_m \quad \text{such that} \\ (3.9d) & \\ (3.9e) & \end{aligned} \quad \left\{ \begin{array}{l} \tilde{f}(x, \bar{p}_0, \delta) = 0, \\ \det(I - M_{J_{11}}^\epsilon \Delta) = 0, \\ -k_m \leq \delta_i \leq k_m, \\ \tilde{f}((1 + \epsilon_x)x, \bar{p}_{\epsilon_p}, \delta) = 0, \\ \det(I - M_{J_{11}}^\epsilon \Delta^\epsilon) = 0, \end{array} \right.$$

578

$$579 \quad X = [x; \delta; \omega; \epsilon_\nu; \epsilon_x; \epsilon_\omega], \quad n_{ctrs} = n_x + 2 + n_\delta + n_x + 2.$$

580 The first set of constraints (3.9a-3.9c) is identical to those in Program 3.2. The  
 581 constraints (3.9d-3.9e) instead ensure that the Jacobian linearized at  $\bar{p}_{\epsilon_p}$  has an ei-  
 582 genvalue  $\nu^\epsilon$  with real part  $\epsilon_\nu$  (3.8d). Making use of a finite difference approximation,  
 583 it follows from the definition in (2.2) that  $l_0 = \frac{\epsilon_\nu}{\epsilon_p}$ . Therefore, existence of a solution  
 584 to Program 3.3 with  $\hat{\epsilon}_\nu \neq 0$  guarantees a Hopf bifurcation for the system.

585 Underlying Program 3.3 there is a perturbation argument which builds on the  
 586 application of the IFT to the states  $x$  and the eigenvalue  $\nu$  of the vector field  $\tilde{f}(x, p, \hat{\delta})$   
 587 for fixed  $\hat{\delta}$  and  $p$  in a neighbourhood of  $\bar{p}_0$ . Indeed, at  $p = \bar{p}_0$ , it holds  $x = \hat{x}$  and  
 588  $\nu = i\hat{\omega}$  for the constraints (3.9a-3.9c). When perturbing  $p$  by a small increment  $\epsilon_p$ ,  
 589 a first order approximation for  $x$  and  $\nu$  is assumed, and reflected in the choice of the  
 590 scalars  $\epsilon_x$  (3.8c), as well as  $\epsilon_\omega$  and  $\epsilon_\nu$  (3.8d). A vector  $\epsilon_x$ , with an element for each  
 591 component of  $x$ , could also be considered, by adding  $n_x - 1$  unknowns to Program 3.3.

592 *Remark 3.2.* Program 3.2 does not mathematically guarantee the onset of a Hopf  
 593 bifurcation because it does not take into account the transversality condition, and  
 594 for this reason Program 3.3 is proposed. However, for engineering systems where  $p$   
 595 has a physical meaning (e.g., load power in a power system, speed for an aircraft)  
 596 the transversality condition is often automatically verified. In fact, cases where this  
 597 condition is not satisfied are termed *degenerate* in the literature [18]. For this reason,  
 598 the problem was stated in Sec. 3.1 assuming that the nominal system has a bifurcation  
 599 at  $p_H$  whereas for  $p = \bar{p}_0$  the system has a stable equilibrium. It is thus implicit in  
 600 the formulation of the problem that a change of  $p$  has an effect on the stability of  
 601 the system. In particular, it is expected that the critical eigenvalues of the perturbed  
 602 Jacobian will cross the imaginary axis as  $p$  is perturbed around  $\bar{p}_0$ .

603 It is observed that, compared to Program 3.2, Program 3.3 only adds three unknowns  
 604 to the vector of optimization variables  $X$ , and has  $n_x + 2$  additional constraints.  
 605 Its effect in terms of computational cost is thus not expected to be important.

606 However, a strong reason to resort to Program 3.2 whenever possible is related to  
 607 the local optimality of the solutions of nonlinear programs. This issue will be further  
 608 discussed in Sec. 3.3, but it is remarked here that the addition of the constraints  
 609 (3.9d-3.9e) has a detrimental effect on it. Indeed it is always advisable in nonlinear  
 610 optimization to avoid redundant constraints in order to reduce the likelihood of local  
 611 optima [33]. Based on these considerations, and the discussion in Remark 3.2, the  
 612 proposed strategy is to employ Program 3.2 to find robust bifurcation margins and, if  
 613 continuation analyses of the perturbed system show that the transversality condition  
 614 is not fulfilled, use Program 3.3. It is noted that none of the analyses done in support  
 615 of this study required the adoption of Program 3.3 (which however was tested to verify  
 616 its soundness). For this reason, and also for the sake of clarity, in the remainder of the  
 617 work Program 3.2 will be considered as the basis for discussion and further algorithms.

### 618 Specifying the type of closest Hopf bifurcation

619 The robust bifurcation margin  $k_m$  has been associated so far with the occur-  
 620 rence of a generic Hopf bifurcation. Attention is now focused on the nature of the  
 621 bifurcation, i.e., subcritical or supercritical. The idea is to add a condition on the  
 622 sign of the Lyapunov coefficient  $l_1$  to the constraints of Program 3.2. This can be  
 623 done by using the definition of  $l_1$  (2.4), which requires the computation of left and  
 624 right eigenvectors associated with the critical eigenvalue, and the tensors of second  
 625 and third order derivative. By exploiting the fact that  $\omega$  is an optimization variable,  
 626 the eigenvectors can be computed without performing an eigenvalue analysis, but by



627 direct computation as follows

$$\begin{aligned}
 & (\tilde{J} - i\omega I_{n_x})q = 0, \quad q = [1; q_l], \\
 628 \quad (3.10) \quad & (\tilde{J}^T + i\omega I_{n_x})r = 0, \quad r = [1; r_l], \\
 & \langle r, q \rangle = 1,
 \end{aligned}$$

629 where without loss of generality the first element of the eigenvectors has been fixed  
 630 to 1. As for the tensors, the derivatives in (2.6) can be computed analytically in  
 631 simple cases and by automatic or symbolic differentiation for more complex ones.  
 632 Alternatively, in [27] efficient strategies to avoid computing second and third order  
 633 derivatives of the vector field are discussed. In any case, they are available as a  
 634 function of the optimization variables  $x$  and  $\delta$ , and thus the only addition to the  
 635 vector of unknowns  $X$  is essentially  $l_1$ .

636 In conclusion, given a positive tolerance  $\epsilon_l$  on the value of the Lyapunov coefficient,  
 637 and an integer  $s_l = \pm 1$  defining the sign of  $l_1$  ( $s_l = 1$  for subcritical and  $s_l = -1$   
 638 for supercritical), the following program allows the closest subcritical or supercritical  
 639 Hopf bifurcation to be computed.

PROGRAM 3.4.

$$\begin{aligned}
 (3.11a) \quad & \tilde{f}(x, \bar{p}_0, \delta) = 0, \\
 (3.11b) \quad & \det(I - M_{\bar{J} \ 11} \Delta) = 0, \\
 (3.11c) \quad & \min_X k_m \quad \text{such that} \quad \begin{cases} -k_m \leq \delta_i \leq k_m, & i = 1, \dots, n_\delta, \\ (3.11d) \quad s_l l_1 - \epsilon_l > 0, \end{cases}
 \end{aligned}$$

640

641

$$X = [x; \delta; \omega; l_1], \quad n_{ctrs} = n_x + 2 + n_\delta + 1.$$

642 To summarize the content of this Section, the problem of computing the closest  
 643 Hopf bifurcation point in the uncertain parameter space has been formulated via  
 644 a nonlinear optimization problem and has been presented incrementally in order to  
 645 stress the key steps involved. Because the Hopf bifurcation can be of two types, namely  
 646 subcritical and supercritical, two Programs are proposed. Program 3.2 determines  
 647 the closest Hopf bifurcation to a given stable equilibrium (this might be subcritical or  
 648 supercritical, depending on the specific case), whereas Program 3.4 allows the type of  
 649 closest Hopf bifurcation (via a constraint on the Lyapunov coefficient) to be specified.  
 650

651 **3.3. Continuation-based multi-start strategy.** The programs discussed in  
 652 Section 3.2 allow margins to Hopf bifurcation for a nominally stable equilibrium point  
 653 in the face of uncertainties to be computed. The main issue with this approach is  
 654 that, due to the fact that is based on nonlinear optimization, there is no guarantee  
 655 that the one found is the closest bifurcation, and thus in practice only upper bounds  
 656 on  $k_m$  are computed. In other words, global minima might be missed and thus there  
 657 could be a vector  $\bar{\delta}$  featuring a smaller norm than  $\hat{\delta}$  which causes a Hopf bifurcation.  
 658 Local optima are a well known issue in nonlinear optimization and, while there exist  
 659 global optimization algorithms that can guarantee global optima, their computational  
 660 burden grows exponentially with the dimension of the problem and thus often are not  
 661 practical solutions [33].

662 Mitigation strategies when local solvers (e.g. interior point methods) are used  
 663 depend on several aspects, including specific features of the program (e.g., objective  
 664 functions) and adopted optimization algorithms [17]. For this problem the objective

665 is to compute worst-case perturbations quantified by means of a scalar metric, thus a  
666 possible way to account for this issue is to estimate a guaranteed smallest magnitude  
667 of the perturbation for which the system is stable. This is the approach taken in  $\mu$   
668 analysis, where the computation of  $\mu_{LB}$  is known to be prone to local minima and as  
669 a remedy upper bounds  $\mu_{UB}$  have been proposed. Lower bounds on  $k_m$  (nonlinear  
670 analogs of  $\mu_{UB}$ ) could then be a strategy in the present context, but this has not been  
671 pursued here and could be a topic of future research.

672 As for the optimization algorithms, the focus of this work is not on developing  
673 ad-hoc advanced optimization strategies, hence off-the-shelf algorithms available in  
674 MATLAB for nonlinear constrained problems are employed [31]: These include: *in-*  
675 *terior point*, which solves the constrained problem using a sequence of unconstrained  
676 optimizations by using barrier or penalty functions to account for the constraints;  
677 *active set* and *sqp*, belonging to the class of sequential quadratic programmes, which  
678 directly solve the constrained problem via a series of approximating quadratic pro-  
679 gramming based on the Karush-Kuhn-Tucker equations (necessary conditions for op-  
680 timality of constrained optimization problems). Leveraging the availability of solvers  
681 based on different optimization methods, a (naive but possible) strategy employed in  
682 the work is to restart the programs using different solvers.

683 Another good practice to reduce the likelihood of local minima is to formulate the  
684 problem in the *simplest* way possible [33], e.g., using smooth objective functions and  
685 constraints and avoiding redundant constraints. These two principles have guided  
686 the idea of introducing the objective function  $k_m$  to relax the non-smooth bound  
687 on the uncertainty set involving  $\bar{\sigma}$ , which lead to the equivalent constraints (3.6).  
688 Moreover, the aim of simplifying as much as possible the set of constraints prompted  
689 the discussion in Remark 3.2, where it was proposed (based on a physically moti-  
690 vated assumption) to resort to Program 3.3 only if the solution does not satisfy the  
691 transversality condition.

692 A strategy which exploits a distinctive feature of this formulation is to run Pro-  
693 gram 3.2 at a given frequency, i.e.,  $\omega$  does not belong to  $X$  but is fixed a priori. The  
694 rationale behind this is twofold. From a mathematical point of view, the optimization  
695 is simplified by the fact that constraint (3.7b) does not depend on the frequency and  
696 this enhances the accuracy of the result. From a bifurcation perspective, fixing the  
697 frequency restricts the mechanisms by which the system can undergo a Hopf bifur-  
698 cation when subject to uncertainties, which reduces the number of feasible solutions  
699 in the first place, and as a result makes it also more likely to detect the optimal one.  
700 A value of  $k_m$  can be associated with each discrete frequency, and the smallest of  
701 these values can be regarded as the most critical. A natural drawback of this ap-  
702 proach is that critical frequencies can be missed, but this can be overcome by running  
703 Program 3.2 in a second step with  $\omega$  as optimization variable and initializing it with  
704 values corresponding to the critical solution.

705 Despite these measures, the risk of falling into local minima is still present.  
706 In particular, the programs' initialization represents a critical aspect and thus a  
707 continuation-based multi-start strategy is proposed. Assume that the optimizer has  
708 found a solution  $\hat{X}$  to Program 3.2. The goal is then to provide the optimizer with a  
709 set of initializations, derived from  $\hat{X}$  but possibly not leading the optimizer to find the  
710 same solution, which allows an exhaustive optimization campaign to be performed.  
711 The following extended continuation problem based on the constraints of Program 3.2

712 is first considered

$$713 \quad (3.12) \quad F(x, \delta, \omega, \lambda_d, \lambda_k) = \begin{pmatrix} \tilde{f}(x, \bar{p}_0, \delta) \\ \det(I - M_{\bar{J}_{11}} \Delta) \\ \bar{\sigma}(\Delta_u) \end{pmatrix} - \begin{pmatrix} 0 \\ \lambda_d \\ \lambda_k \end{pmatrix} = 0.$$

714 This can be recast in the formalism of (2.7) by setting

$$715 \quad (3.13) \quad \begin{aligned} u &= X = [x; \delta; \omega], \quad u \in \mathbb{R}^{n_u}, \quad n_u = n_x + n_\delta + 1, \\ \lambda &= [\lambda_d; \lambda_k], \quad \lambda_d \in \mathbb{R}^2, \quad \lambda_k \in \mathbb{R}^1, \\ \Phi &= \tilde{f}(x, \bar{p}_0, \delta), \quad \Phi : \mathbb{R}^{n_u} \rightarrow \mathbb{R}^{n_x}, \\ \Psi &= [\det(I - M_{\bar{J}_{11}} \Delta), \bar{\sigma}(\Delta_u)], \quad \Psi : \mathbb{R}^{n_u} \rightarrow \mathbb{R}^3, \\ F &: \mathbb{R}^{n_x + n_\delta + 3} \rightarrow \mathbb{R}^{n_x + 3}. \end{aligned}$$

716 Let  $\mathbb{I} = \{1, 2\}$  and  $\bar{\mathbb{I}} = \{3\}$  be its complement, with  $\lambda_{\mathbb{I}} = \{\lambda_i | i \in \mathbb{I}\}$  and  $\lambda_{\bar{\mathbb{I}}} = \{\lambda_i | i \in \bar{\mathbb{I}}\}$ , and  $u^* = \hat{X}$ ,  $\lambda^* = \Psi(u^*)$ . By construction, the restriction  $F(u^*, \lambda)|_{\lambda_i = \lambda_i^*} = 0$   
717 and  $F(u, \lambda)|_{\lambda_i = \lambda_i^*}$  satisfies the IFT at  $(u^*, \lambda^*)$ . Therefore,  $F(u, \lambda)|_{\lambda_i = \lambda_i^*}$  defines a  
718 continuation problem for the  $d$ -manifold with  $d = n_x + n_\delta + 1 - (n_x + 2) = n_\delta - 1$ .  
719 Note that  $\lambda_{\mathbb{I}}$  (coinciding with  $\lambda_d$ ) are inactive continuation parameters (corresponding  
720 to active constraints) because they are kept constant during continuation and they  
721 ensure the singularity of the LFT  $\mathcal{F}(M_{\bar{J}}, \Delta)$ . Since  $\lambda_d^* = 0$ , the corresponding active  
722 constraints could have been equivalently embedded in the zero function  $\Phi$  but, for  
723 consistency with the parallel between  $f$  and  $\Phi$  discussed in Sec. 2.1.2, this has been  
724 used for the vector field only. On the other hand,  $\lambda_{\bar{\mathbb{I}}}^*$  (i.e.,  $\lambda_k$ ) corresponds to an  
725 inactive monitor function bookkeeping the magnitude of the perturbation at each  
726 step of the continuation.  
727

728 The manifold associated with (3.12), denoted here by  $\mathcal{H}$ , represents the set of Hopf  
729 bifurcation points *connected* to the solution  $\hat{X}$  in the uncertain parameter space. A  
730 first important observation is that the dimension of  $\mathcal{H}$  is  $n_\delta - 1$ . This is in agreement  
731 with the well known fact [3] that a branch (i.e., 1-dimensional manifold) of Hopf  
732 points can be obtained by continuing simultaneously two parameters starting from a  
733 known initial point. Indeed, in the case of two uncertainties ( $n_\delta = 2$ )  $\mathcal{H}$  is the branch  
734 of Hopf points connected to the initial solution  $\hat{X}$ .

735 In principle, the computation of  $\mathcal{H}$  could directly locate bifurcation points associ-  
736 ated with perturbations featuring a smaller magnitude than  $\hat{\delta}$  by monitoring  $\lambda_k$  (note  
737 however that they could still be local optima since only the connected branches can  
738 be tracked). In addition to that, exploring the *surroundings* of  $\hat{X}$  (using a continua-  
739 tion meaning of this terminology) can provide the sought initialization points for a  
740 new optimization campaign. Unfortunately,  $\mathcal{H}$  is generally multidimensional. In fact,  
741 it is reasonable to assume that even for a relatively small number of uncertainties  
742 computing  $\mathcal{H}$  is not viable. To overcome this, a 1-dimensional restriction of  $\mathcal{H}$  is  
743 constructed by considering a parametrization of the uncertainty set  $\delta$  with a vector  
744 function  $g(z, y) : \mathbb{R}^2 \rightarrow \mathbb{R}^{n_\delta}$ , where the 2 independent variables  $z$  and  $y$  have been  
745 introduced. The definition of  $g$  is arbitrary and various strategies can be pursued.  
746 The approach taken here assumes that two solutions  $\hat{X}^1$ , and  $\hat{X}^2$  from Program 3.2  
747 are available (their selection will be commented on later). Given the associated per-

748 perturbation vectors  $\hat{\delta}^1$ , and  $\hat{\delta}^2 \in \mathbb{R}^{n_\delta}$ , a possible choice for  $g$  is then

$$749 \quad (3.14) \quad g(z, y) : \mathbb{R}^2 \rightarrow \mathbb{R}^{n_\delta} \begin{cases} \hat{\delta}_1^1 z + \hat{\delta}_1^2 (1 - y), \\ \dots \\ \hat{\delta}_i^1 z + \hat{\delta}_i^2 (1 - y), \\ \dots \\ \hat{\delta}_{n_\delta}^1 z + \hat{\delta}_{n_\delta}^2 (1 - y), \end{cases}$$

750 Note that by construction  $g(1, 1) = \hat{\delta}^1$  and  $g(0, 0) = \hat{\delta}^2$ .

751 Based on this, the following continuation problem is formulated

$$752 \quad (3.15) \quad F(x, \delta, \omega, z, y, \lambda_d, \lambda_k, \lambda_g) = \begin{pmatrix} \tilde{f}(x, \bar{p}_0, \delta) \\ \det(I - M_{\bar{J}} \Delta) \\ \bar{\sigma}(\Delta_u) \\ \delta - g(z, y) \end{pmatrix} - \begin{pmatrix} 0 \\ \lambda_d \\ \lambda_k \\ \lambda_g \end{pmatrix} = 0.$$

753 With respect to the definitions in (3.13),  $z$  and  $y$  have been added to the vector of  
754 continuation variables  $u$  (i.e.,  $u = [X; z; y]$ ), while the vector function  $\delta - g$  has been  
755 added to the family of monitor functions  $\Psi$  (with associated continuation parameters  
756  $\lambda_g \in \mathbb{R}^{n_\delta}$ ).

757 Let  $\mathbb{I} = \{1, 2, 4, \dots, 4 + n_\delta\}$ , and  $\bar{\mathbb{I}}$ ,  $\lambda_{\bar{\mathbb{I}}}$ ,  $\lambda_{\bar{\mathbb{I}}}$  as before. Two starting points are  
758 available, respectively  $u^* = [\hat{X}^1; 1; 1]$  and  $u^* = [\hat{X}^2; 0; 0]$ , with  $\lambda^* = \Psi(u^*)$ . Note that  
759 in both cases  $\lambda_g^* = \Psi(u^*) = 0$  by construction. Therefore,  $\delta = g(z, y)$  at each step of  
760 the continuation, and  $\delta$  is expressed as a linear combination of  $\hat{\delta}^1$  and  $\hat{\delta}^2$ .

761 Since  $F(u^*, \lambda)|_{\lambda_{\mathbb{I}}=\lambda_{\mathbb{I}}^*} = 0$  and  $F(u, \lambda)|_{\lambda_{\mathbb{I}}=\lambda_{\mathbb{I}}^*}$  satisfies the IFT at  $(u^*, \lambda^*)$ , then  
762 a manifold  $\mathcal{H}_g$  with dimension  $d = n_x + n_\delta + 3 - (n_x + 2 + n_\delta) = 1$  is defined.  
763 Crucially, the dimension is 1 irrespective of the number of uncertainties  $n_\delta$ , with the  
764 drawback that these are now constrained to vary according to (3.14).  $\mathcal{H}_g^1$  and  $\mathcal{H}_g^2$   
765 indicate the manifold built starting from  $[\hat{X}^1; 1; 1]$  and  $[\hat{X}^2; 0; 0]$  respectively, with  
766 the subscript and the superscript highlighting the dependence on the parametrization  
767 of the uncertainties  $g$  and the initial point.

768 The construction of  $\mathcal{H}_g$  requires two perturbation vectors  $\hat{\delta}^1$  and  $\hat{\delta}^2$ . This is not  
769 restrictive, since as a result of the local optimality typically more than one solution  
770 is available. In addition, the possibility of running the optimization at a fixed fre-  
771 quency  $\omega$  can be advantageously exploited with the goal of obtaining different *modes*  
772 of perturbations. Indeed, as discussed before, Hopf bifurcations occurring at different  
773 frequencies could represent different mechanisms underlying the loss of stability, thus  
774 considering a linear combination of the perturbations as in (3.14) represent an efficient  
775 strategy to select points on  $\mathcal{H}_g$ .

776 To sum up the multi-start strategy approach, the starting point is **Program 3.2**  
777 which provides a solution consisting of an equilibrium point  $\hat{x}$  of  $f$  perturbed by  $\hat{\delta}$  such  
778 that the associated Jacobian  $\bar{J}$  has a pair of purely imaginary eigenvalues. This is not  
779 necessarily the closest bifurcation point to the nominal system due to the possibility  
780 of local minima. However,  $\hat{X}$  can be used to compute the restricted manifold  $\mathcal{H}_g$  via a  
781 numerically *cheap* continuation problem once a parametrization  $g$  for the uncertainty  
782 set is provided. Continuation of  $\mathcal{H}_g$  has two objectives. First, it could directly detect  
783 improved solutions of **Program 3.2** (if  $\lambda_k < \hat{k}_m$ ). Second, points on  $\mathcal{H}_g$  can be used  
784 to run **Program 3.2** with different initializations.

785 If the manifold  $\mathcal{H}_g$  gathers a large number of points, and running the optimization  
786 for each of them is not viable, criteria could be employed to select a subset of them

787 only. Keeping in mind that the goal is to provide initializations which possibly make  
 788 the optimizer converge to different points from the initial solution  $\hat{X}$ , the premise  
 789 of these criteria is to detect on  $\mathcal{H}_g$  perturbation vectors *qualitatively* different from  
 790  $\hat{\delta}$ . Possible indicators are for example the frequency  $\omega$  and the changes in sign of  
 791 the parameters in  $\delta$  (recall that these are normalized, thus a change in sign reveals a  
 792 change in the direction of perturbation for the considered parameter).

793 **3.4. Comparison with the direct method.** The framework presented in the  
 794 previous sections allows the computation of the robust bifurcation margin  $k_m$  via  
 795 nonlinear optimization (section 3.2) aided by a multi-start strategy (3.3). Despite its  
 796 importance for the analysis of nonlinear systems, the computation of the closest Hopf  
 797 bifurcation point to a stable equilibrium in the uncertain parameter space has not  
 798 been adequately investigated so far. The only alternative approach available in the  
 799 literature is the so-called *direct* method [12], and the objective of this section is to  
 800 point out the differences (and the associated advantages) of the formulation proposed  
 801 in this paper (in the remainder of this section termed *margin* method) with respect  
 802 to it.

803 The direct method for Hopf bifurcations considers as starting point the vector  
 804 field (2.1) where  $n_p > 1$ , i.e. the vector of bifurcation parameters is multidimensional.  
 805 Given a vector  $\bar{p}_0$  associated with a stable equilibrium, the closest point to  $\bar{p}_0$  in the  
 806 set of parameters (or hypersurface)  $\Sigma$  for which the equilibrium experiences a Hopf  
 807 bifurcation is sought. A first difference is thus that in the margin method a distinction  
 808 is drawn between bifurcation parameter  $p$  (of dimension equal to the codimension of  
 809 the bifurcation, which is 1 for the Hopf case) and uncertain parameters  $\delta$ , and the  
 810 closest Hopf point is sought in the uncertainty space only (that is,  $\bar{p}_0$  is fixed). Con-  
 811 versely, in the direct method bifurcation and uncertain parameters are all gathered  
 812 in  $p$  and can all be perturbed in order to reach the closest bifurcation point. This  
 813 difference only pertains to the formulation of the problem, but it is worth highlighting  
 814 it since two different perturbation scenarios are effectively considered.

815 The key observation leveraged by the direct method is that if  $p_*$  is the closest point  
 816 to  $\bar{p}_0$  in  $\Sigma$ , then the vector  $p_* - \bar{p}_0$  is parallel to the normal vector to the hypersurface  
 817  $\Sigma$  at  $p_*$ . Moreover,  $p_*$  is a *local* minimum if the distance  $|p_* - \bar{p}_0|$  is smaller than the  
 818 reciprocal of the curvature of  $\Sigma$  at  $p_*$ .

819 Implementation of these conditions lead to the extended system of equations defining  
 820 a Hopf bifurcation ([12], Section 5). The name *extended* derives from the fact that, for  
 821  $n_p = 1$ , this set of equations reduces to the standard system of equations to compute  
 822 Hopf bifurcation branches (Th. 2.1). The multidimensional case exploits the fact that  
 823 the normal vector at  $p_*$  can be written out as a function of  $\nabla_p f|_{p=p_*}$  and of the eigen-  
 824 vector of the Jacobian  $\nabla_x f|_{p=p_*}$  associated with the purely imaginary eigenvalues.  
 825 In turn, the curvature can be written as a function of the normal vector. Building  
 826 on these relationships and enforcing all the associated constraints, the problem is fi-  
 827 nally formulated as the solution of  $6n_x + n_p + 2$  nonlinear equations in  $6n_x + n_p + 2$   
 828 unknowns. Similarly to the margin method (see the vector  $X$  in Program 3.2), the  
 829 unknowns of the problem include the perturbed equilibrium ( $n_x$ ), the closest bifur-  
 830 cation parameter vector ( $n_p$ ), and the frequency (1). However, in addition to these  
 831 there are another  $5n_x + 1$  unknowns which are introduced in order to express the rest  
 832 of the constraints, and clearly do not feature in the margin method. The key ideas  
 833 leveraged by the margin method to avoid these additional constraints are to enforce  
 834 the constraint on the Jacobian as singularity of the LFT (3.7b) and cast the minimum  
 835 distance problem as maximum singular value minimization of the perturbation matrix

836  $\Delta$ . As for the number of constraints, [Program 3.2](#) has  $n_{ctrs} = n_x + 2 + n_\delta$  while the  
 837 direct method features  $6n_x + n_p + 2$ . A comparison in terms of size of the problem,  
 838 both in terms of unknowns and constraints, points out an objective advantage of the  
 839 margin method with respect to the direct method. Quoting the author in [12], “*this*  
 840 *direct method for computing Hopf bifurcations may be too cumbersome to be useful if*  
 841  *$n_x$  is large”.*

842 The distinctions between the two methods are however not restricted to the size of the  
 843 problem. For example, the mathematical formulation of the problem is different. In  
 844 the margin method,  $k_m$  is the result of an optimization problem whereas in the direct  
 845 method a determined (the number of constraints equals the number of unknowns) set  
 846 of nonlinear equations has to be solved (e.g. with Newton-type methods). This is  
 847 deemed an advantage of the margin method, since the greater degree of freedom in  
 848 finding the solution can be exploited using optimization techniques in order to achieve  
 849 higher efficiency in the computation and more robustness to the problem of local min-  
 850 ima. As for the latter aspect, it is further observed that the margin method is also  
 851 equipped with the multi-start strategy (3.3), as opposed to the direct method where  
 852 there are no strategies to directly tackle the problem of converging to local minima.

853 Another favourable feature offered by the margin method is that it allows the type  
 854 of closest bifurcation to be specified via constraint on the Lyapunov coefficient ([Pro-  
 855 gram 3.4](#)). This is done in a relatively straightforward way by using the fact that  $\omega$   
 856 is an optimization variable, and thus the eigenvectors needed for the computation of  
 857  $l_1$  (2.4) are available without performing an eigenvalue analysis (3.10). As a result,  
 858 [Program 3.4](#) only adds one unknown ( $l_1$ ) and one scalar constraint to [Program 3.2](#)  
 859 where the type of bifurcation is not specified. This is again due to the LFT formula-  
 860 tion of the problem that provides an analytic dependence of the constraints on  $\omega$  (see  
 861 also Remark 3.1). Conversely, the option of specifying the closest bifurcation is not  
 862 available in the direct method, nor is it clear how it could be added without incurring  
 863 a further substantial increase in the number of unknowns and constraints.

864 Another important aspect is related to the type of constraints involved in the two  
 865 problems. As discussed in Remark 3.1, the gradients of the constraints in [Program 3.2](#)  
 866 with respect to the unknowns (with the exception of  $\omega$ , which is more tedious) can all  
 867 be analytically computed and provided to the solver, with great advantage in terms  
 868 of efficiency of computation. This clearly does not apply to the direct method due  
 869 to the very complicated definition of the constraints (involving eigenvectors and their  
 870 projections) and of the unknowns.

871 Finally, a unique feature of the robust bifurcation margin  $k_m$  owes to its interpre-  
 872 tation as nonlinear extension of the structured singular value  $\mu$ . This indeed opens  
 873 up the possibility to transfer to the bifurcation field many of the well established  
 874 approaches in robust control [48]. This applies to: modelling, where advanced LFT  
 875 algorithms [28, 29] can be employed to efficiently formulate the constraints of [Pro-  
 876 gram 3.2](#) and [Program 3.4](#); analysis, where the insightful interpretations of  $\mu$  and  
 877 associated analysis strategies (sensitivity, frequency-domain analysis) [26] carry over  
 878 to  $k_m$ ; and ultimately robust control design, whereby a (potentially nonlinear) con-  
 879 troller is synthesised to prevent bifurcations in the face of a given uncertainty set.  
 880 While examples of the first two aspects have been given throughout the section and  
 881 will be exemplified further in [section 4](#), the latter is an exciting prospective line of  
 882 research that can build on this initial work.

883 **4. Numerical examples.** The proposed concept of robust bifurcation margin  
 884 is demonstrated on two test cases from the literature. The first is a power system

885 model for which the sensitivity of the Hopf bifurcation to modeling parameters was  
 886 considered in [13], while the second is an aeroelastic case study previously studied  
 887 with linear robust control techniques in [25].

#### 888 4.1. Power system.

889 **4.1.1. Model description.** The first example considers the single machine  
 890 power load system with voltage regulator and dynamic load model studied in [13]  
 891 and depicted in Fig. 4. The model used in [13] is very similar to the one originally  
 892 proposed in [7], with the variations discussed next. The model in [7] consists of: five  
 893 ordinary differential equations representing the dynamics of the generator voltages  
 894  $E'_d + jE'_q$ , the voltage regulator state  $R_f$  and output voltage  $V_R$ , and the field voltage  
 895  $E_{FD}$ ; two algebraic equations which relate the load bus voltage phasor  $V_L/\theta$  to the  
 896 voltage source  $E'_d + jE'_s$  and the load demand  $P_L + jQ_L$ , where  $P_L$  and  $Q_L$  are respec-  
 897 tively the constant (and fixed a priori) active and reactive power components. The  
 898 goal of the regulator is to control the voltage  $E_s$  at the high side of the transformer  
 given a reference voltage setpoint  $E_{ref}$ , which depends on the loading level.

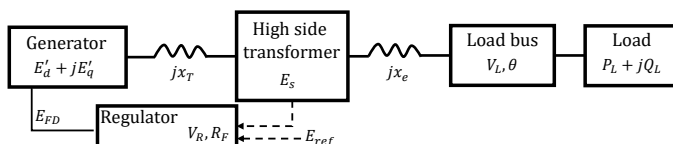


FIG. 4. Power system sketch.

899 Differently from [7], the model in reference [13] considers: a dynamic power load  
 900 (i.e.  $P_L$  and  $Q_L$  are not constant); a setpoint  $E_{ref}$  which is fixed for all loading levels;  
 901 and an expression of the voltage  $E_s$  as a function of the other state variables. Due  
 902 to these changes, two ordinary differential equations are added for  $V_L$  and  $\theta$ , and the  
 903 two algebraic equations become explicit equations for  $P_L$  and  $Q_L$ .

904 The resulting set of seven ordinary differential equations describing the power system,  
 905 with vector of states  $x = [E'_d; E'_q; V_R; E_{FD}; R_f; \theta; V_L]$ , is:

$$907 \quad (4.1a) \quad T'_{q0} \dot{E}'_d = -E'_d + (x_q - x'_d)I_q,$$

$$908 \quad (4.1b) \quad T'_{d0} \dot{E}'_q = -E'_q - (x_d - x'_d)I_d + E_{FD},$$

$$909 \quad (4.1c) \quad T_A \dot{V}_R = -V_R + K_A(E_{ref} - E_s - \frac{K_f E_{FD}}{T_f} + R_f),$$

$$910 \quad (4.1d) \quad T_E \dot{E}_{FD} = -E_{FD} + V_R,$$

$$911 \quad (4.1e) \quad T_f \dot{R}_f = -R_f + \frac{K_f E_{FD}}{T_f},$$

$$912 \quad (4.1f) \quad D\dot{\theta} = P_L - lPF,$$

$$913 \quad (4.1g) \quad k\dot{V}_L = Q_L - l\sqrt{1 - PF^2}.$$

915 where:  $T_{q0}$  and  $T_{d0}$  are the open circuit time constants;  $x_d$  and  $x_q$  are the synchronous  
 916 reactances;  $x'_d$  is the transient reactance;  $I_d$  and  $I_q$  are the currents;  $T_A$  and  $K_A$  are  
 917 the voltage regulator time constant and gain;  $T_E$  is the exciter time constant;  $T_f$  and  
 918  $K_f$  are the time constant and gain of the feedback loop;  $D$  and  $k$  are time constants  
 919 of the load dynamics;  $PF$  is the power factor and  $l$  parameterizes the increase of the

920 constant power part of the load (this will be used as bifurcation parameter in the  
921 analyses).

922 This set of equations must be closed with the defining equations for  $I_d$ ,  $I_q$ ,  $P_L$ ,  $Q_L$ ,  
923 and  $E_s$ . For the currents, the following holds [7]:

$$\begin{aligned}
 I_d &= \frac{1}{x_E} (E'_q - V_L \cos(\delta - \theta)), \\
 I_q &= \frac{1}{x_E} (-E'_d + V_L \sin(\delta - \theta)), \\
 x_E &= x'_d + x_T + x_e.
 \end{aligned}
 \tag{4.2}$$

925 where  $\delta$  is the rotor angle,  $x_T$  is the high side transformer reactance and  $x_e$  is the  
926 transmission line reactance.

927 The equations for the remaining three variables are not provided in [13]. The re-  
928 lationships for  $P_L$  and  $Q_L$  are derived here from the two aforementioned algebraic  
929 equations in [7], which now allow an explicit expression for the load components to  
930 be obtained since the phasor  $V_L/\underline{\theta}$  has a dedicated dynamic description (4.1f-4.1g).  
931 As for  $E_s$ , a relationship to the state variables is derived by considering the loadflow  
932 equation for the circuit with the voltage source at the high side of the transformer.  
933 This leads to:

$$934 \tag{4.3a} \quad P_L = \frac{V_L}{x_E} \cos(\theta) \tilde{P} - \frac{V_L}{x_E} \sin(\theta) \tilde{Q},$$

$$935 \tag{4.3b} \quad Q_L = \frac{V_L}{x_E} \sin(\theta) \tilde{P} + \frac{V_L}{x_E} \cos(\theta) \tilde{Q},$$

$$936 \quad \tilde{P} = -E'_d \cos(\delta) + E'_q \sin(\delta) - V_L \sin(\theta),$$

$$937 \quad \tilde{Q} = E'_d \sin(\delta) + E'_q \cos(\delta) - V_L \cos(\theta),$$

$$938 \tag{4.3c} \quad E_s = \frac{1}{V_L} \sqrt{(x_e P_L)^2 + (x_e Q_L + V_L^2)^2}.$$

940 Note that the same expression for  $E_s$  was used in [46], where a very similar power  
941 system was analyzed.

942 Table 1 reports the values of the parameters used here for the power system  
943 model. These are all taken from [7], except for  $D$  and  $k$  (introduced anew in [13]) and  
944  $K_f$ , whose value was changed in [13]. As for the rotor angle  $\delta$ , it is noted that their  
945 dynamic is assumed faster than the dominant voltage dynamics, thus the angle is in  
946 quasi-steady state and does not have any effect on the results [7]. Time constants are  
in seconds, reactance are p.u. while all the other parameters are dimensionless.

TABLE 1  
*Power system model parameters.*

| $x_T$ | $x_e$ | $x_d$ | $x_q$ | $x'_d$ | $T'_{d0}$ | $T'_{q0}$ | $K_A$ | $T_A$ | $T_E$ | $K_f$ | $T_f$ | $PF$ | $D$  | $k$ |
|-------|-------|-------|-------|--------|-----------|-----------|-------|-------|-------|-------|-------|------|------|-----|
| 0.15  | 0.34  | 1     | 1     | 0.18   | 5         | 1.5       | 30    | 0.4   | 0.56  | 0.1   | 1.3   | 0.95 | 0.05 | 0.1 |

947

948 Numerical continuation is applied to the nominal model using the parameter  $l$  as  
949 bifurcation parameter. The (non-zero) stable equilibrium point at  $l = 0$  is found by  
950 simulating the model and this is provided as an initialization to COCO. The branch  
951 of equilibrium points as  $l$  is increased is reported in Fig. 5 by showing the values of  
952 three components of the state vector, namely  $E'_d$ ,  $R_f$ , and  $V_L$ .



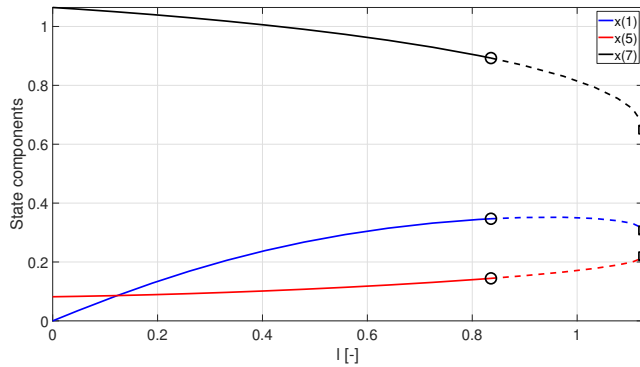


FIG. 5. Bifurcation diagram for the nominal power system model.

953 The analyses show that the system has a branch of stable equilibria for low values  
 954 of  $l$  (this part of the branch is denoted by a solid line), which undergoes a Hopf  
 955 bifurcation at  $l_H=0.83$  (circle marker), with a frequency of the associated imaginary  
 956 eigenvalues equal to  $\omega_H=2.6 \frac{rad}{s}$ , and a saddle node bifurcation at  $l_{SN}=1.13$  (square  
 957 marker). As aforementioned, the model used in here is not exactly the same as that  
 958 of [13] as insufficient information was provided in that reference to reproduce their  
 959 results exactly. In [13], the Hopf bifurcation also occurred at a lower loading level  
 960 than the saddle node one but at different values, i.e.  $l_H=0.37$  and  $l_{SN}=1.03$ . Thus,  
 961 qualitatively speaking, the results from Fig. 5 are similar to those in [13] (see also the  
 962 sensitivity analysis discussed next) and should enable the proposed robust bifurcation  
 963 margin approach to be tested by comparing with the results from [13]<sup>1</sup>.

964 **4.1.2. Sensitivity analysis of the Hopf bifurcation.** The authors in [13]  
 965 compute the sensitivity of both bifurcations to the model's parameters (the focus will  
 966 be here only on the analyses for the Hopf one). This computation is performed by  
 967 first defining what is termed the *loading margin to instability* at  $l_0$  (a value of the  
 968 bifurcation parameter  $l$  corresponding to a stable equilibrium) as  $M(l_0) = l_H - l_0$ .  
 969 The *first-order* sensitivity  $M_c$  of  $M$  to a generic parameter  $c$  (here  $c$  represents any  
 970 model parameter, in the present case those in Table 1) is then computed as the partial  
 971 derivative of  $M$  with respect to  $c$  evaluated at  $l_0$ , i.e.  $M_c(l_0) = \frac{\partial M}{\partial c} \Big|_{l=l_0}$ . Its computa-  
 972 tion is performed using normal vectors to the manifold of Hopf bifurcation points and  
 973 essentially consists of a sensitivity of the critical eigenvalue. An approximation to this  
 974 sensitivity can be computed as  $\tilde{M}_c = \frac{M(l_0, c+\epsilon) - M(l_0, c)}{\epsilon}$ , where  $M(l_0, c + \epsilon) = l_H^{c+\epsilon} - l_0$   
 975 and  $l_H^{c+\epsilon}$  is the value of  $l$  at which a Hopf bifurcation occurs when the parameter  $c$  is  
 976 increased to  $c + \epsilon$ . The quantity  $\tilde{M}_c$  is thus a finite difference approximation of  $M_c$   
 977 and can be computed via numerical continuation. The results of such a sensitivity  
 analysis are reported in Table 2 for the parameters previously listed in Table 1.

TABLE 2  
 Sensitivity of the Hopf bifurcation to model parameters (continuation-based).

|               | $x_T$ | $x_e$   | $x_d$ | $x_q$  | $x'_d$  | $T'_{d0}$ | $T'_{q0}$ | $K_A$ | $T_A$   | $T_E$   | $K_f$ | $T_f$ | $PF$ | $D$    | $k$  |
|---------------|-------|---------|-------|--------|---------|-----------|-----------|-------|---------|---------|-------|-------|------|--------|------|
| $\tilde{M}_c$ | -0.96 | -1.3476 | -0.05 | -0.006 | -0.9111 | 0.039     | 0.0047    | 0.003 | -0.2975 | -0.1982 | 2.1   | -0.14 | 1.5  | -0.005 | 0.11 |

<sup>1</sup>A MATLAB implementation of the power system model presented in this section, together with a file to run continuation analyses with COCO, is available at <https://github.com/AndreaIan/PowerSystem.cont>

978 It is noted that the sign of all the sensitivities (a negative sign means that an  
 979 increase of the parameter makes the loading margin to instability decrease) coincide  
 980 with those reported in [13] except for  $k$ , and the magnitude (proportional to the  
 981 sensitivity to that parameter) is also generally well captured.

982 In order to show the connection between the sensitivity approach used in [13] and  
 983 the concept of robust bifurcation margin, a first type of analysis is discussed next. A  
 984 set of four parameters from the power system model is considered, namely  $x_q$ ,  $K_A$ ,  
 985  $T_A$ , and  $K_f$ . Without loss of generality, only a subset of the parameters in Table  
 986 2 is selected to allow a more clear interpretation of the results. A subcritical value  
 987 of the loading level at which robustness of the plant is studied is then selected; this  
 988 is denoted  $\bar{l}_0$  according to the notation adopted in section 3.1. In all the analyses  
 989 presented here the value  $\bar{l}_0 = 0.725 < l_H$  will be considered. Once the set of uncertain  
 990 parameters and a value of the bifurcation parameter is selected, the corresponding  
 991 LFT can be constructed. It is observed that the dependence of the vector field on the  
 992 states cannot be captured directly in an LFT fashion. This is due to the trigonometric  
 993 functions (4.2-4.3a-4.3b) and square root (4.3c). For this reason, Taylor expansions  
 994 of these functions about the equilibrium state at  $\bar{l}_0$  are considered. The order of the  
 995 expansion (1 and 2 depending on the specific state) is selected in order to guarantee  
 996 a satisfactory trade-off between accuracy and size of the LFT  $\mathcal{F}(M_{\bar{j}}, \Delta)$ . For all  
 997 the uncertain parameters a range of variation of  $\pm 15\%$  from the nominal value is  
 998 considered.

999 Program 3.2 is employed with an initialization provided by the nominal values of  
 1000 the equilibrium point and of the uncertainties. The value of the Lyapunov coefficient  
 1001  $l_1$  will not be considered as a variable in these analyses since the goal is not to study  
 1002 the effect of the parameters on the type of Hopf bifurcation, even though this would  
 1003 also be possible within this framework. Five different tests will be considered: four in  
 1004 which only one parameter belongs to the uncertainty set  $\Delta_u$  (the total size of each of  
 1005 the four LFTs is 17), and one in which all the four parameters are included in  $\Delta_u$  (the  
 1006 total size of the LFT is 25). The results are reported in Table 3 in terms of robust  
 1007 stability margin  $k_m$ , frequency  $\hat{\omega}$  and worst-case perturbation for the normalized  
 1008 uncertainties.

TABLE 3  
*Sensitivity analysis with the robust bifurcation margin at  $\bar{l}_0 = 0.725$ .*

| test | $k_m$    | $\hat{\omega} \frac{rad}{s}$ | $\delta_{x_q}$ | $\delta_{K_A}$ | $\delta_{T_A}$ | $\delta_{K_f}$ |
|------|----------|------------------------------|----------------|----------------|----------------|----------------|
| 1    | 24.3     | 2.3                          | 24.3           | .              | .              | .              |
| 2    | $\infty$ | n.a.                         | .              | n.a.           | .              | .              |
| 3    | 7.8      | 2.1                          | .              | .              | 7.8            | .              |
| 4    | 2.5      | 2.6                          | .              | .              | .              | -2.5           |
| 5    | 1.54     | 2.2                          | 1.54           | -1.54          | 1.54           | -1.54          |

1009 The value of  $k_m$  for the first four tests, where only one parameter at a time  
 1010 is allowed to vary, can be considered as a measure of the sensitivity of the Hopf  
 1011 bifurcation to that parameter –and it is thus expected to show similar results to  
 1012 those obtained in [13]. Indeed, all the predictions reported in Table 2 (which was in  
 1013 agreement with [13]) are confirmed: high sensitivity to  $K_f$ , medium sensitivity to  $T_A$ ,  
 1014 and practically no sensitivity to  $x_q$  and  $K_A$  (note that for the latter the optimization  
 1015 problem was found infeasible). Moreover, the signs of the worst-case perturbations  
 1016 are also in agreement with the findings in Table 2. The fifth test shows that when

1017 all the parameters are acting together the margin  $k_m$  decreases, but it is still greater  
 1018 than 1, that is the power system at  $\bar{l}_0$  is robust to the uncertainty considered. For the  
 1019 predicted worst-case perturbation, the Hopf bifurcation taking place at  $\bar{l}_0$  is associated  
 1020 with a frequency  $\hat{\omega} = 2.2 \frac{rad}{s}$  (recall that this is one of the optimization variables of  
 1021 [Program 3.2](#)), which is smaller than the one in the nominal case, but within the same  
 1022 frequency range.

1023 While the proposed robust bifurcation margin framework can be used to retrieve  
 1024 the results of the sensitivity tests performed in [\[13\]](#), one of its advantage is that allows  
 1025 also for another type of sensitivity analysis. In particular, the effect of a parameter  
 1026 on the bifurcation is evaluated while simultaneously accounting for the other uncer-  
 1027 tainties affecting the system. This is inherently different from the sensitivity measure  
 1028 proposed in [\[13\]](#), which is a first-order approximation of the partial derivative of the  
 1029 margin, and thus effectively neglects any coupling among the uncertainties. This key  
 1030 aspect will be exemplified with a second type of  $k_m$ -based analysis.

1031 It is known that the structured singular value  $\mu$  can be used to evaluate the  
 1032 sensitivity of an instability to a set of  $n_\delta$  selected parameters by performing multiple  
 1033  $\mu$  tests. This can be achieved for example using the skew- $\mu$  concept [\[30\]](#), or, within  
 1034 standard  $\mu$  analysis tools, by considering two different uncertainty levels  $w_{1,d_i}$  and  
 1035  $w_{2,d_i}$  (recall the definition of the uncertainty level in [Eq. 3.3](#)) for each parameter  $d_i$   
 1036 ( $i = 1, \dots, n_\delta$ ). In the first  $\mu$  test (termed *base* to indicate it is the baseline test), all  
 1037 the parameters have the uncertainty level  $w_{1,d_i}$ , while in the following  $n_\delta$  tests, the  
 1038 uncertainty level of the  $i$ -th parameter is set to  $w_{2,d_i}$  and for all the others it is kept  
 1039 at  $w_{1,d_j}$  (with  $j \neq i$ ). The difference between the peak of the baseline  $\mu$  plot and  
 1040 the peaks of the other  $n_\delta$  tests is proportional to the sensitivity of the instability to  
 1041 the considered parameter. See [\[26\]](#) for an application of this analysis approach to the  
 1042 robust flutter problem.

1043 In the same spirit, the parameters studied in [Table 3](#) are analyzed here considering  
 1044  $w_1 = 0.15$  (i.e the previously defined 15% uncertainty range) and  $w_2 = 0.3$  (i.e.  
 1045 doubling the range for the specific parameter used in the  $n_\delta$  test). [Program 3.2](#)  
 1046 is again employed and the results are shown in [Table 4](#) (the first column identifies the  
 1047 test performed, i.e. *base* and then the parameter whose uncertainty level is set to  $w_2$ ).

TABLE 4  
 Robust bifurcation margin sensitivity analysis at  $\bar{l}_0 = 0.725$ .

| test  | $k_m$ | $\hat{\omega} \frac{rad}{s}$ | $\delta_{x_q}$ | $\delta_{K_A}$ | $\delta_{T_A}$ | $\delta_{K_f}$ |
|-------|-------|------------------------------|----------------|----------------|----------------|----------------|
| base  | 1.54  | 2.2                          | 1.54           | -1.54          | 1.54           | -1.54          |
| $x_q$ | 1.41  | 2.2                          | 1.41           | -1.41          | 1.41           | -1.54          |
| $K_A$ | 1.31  | 2                            | 1.31           | -1.31          | 1.31           | -1.31          |
| $T_A$ | 1.24  | 2.2                          | 1.24           | -1.24          | 1.24           | -1.24          |
| $K_f$ | 0.97  | 2.4                          | 0.97           | -0.97          | 0.97           | -0.97          |

1048

1049 The baseline test coincides with test 5 in [Table 3](#) but is reported to facilitate  
 1050 the comparison. The different sensitivity of the considered parameters is confirmed  
 1051 in this new analysis (from the least sensitive parameter  $x_q$  to the most sensitive one  
 1052  $K_f$ ). However, it is also clear that every parameter now has an effect on the shift of  
 1053 the bifurcation point towards  $\bar{l}_0$ . This is clearly seen comparing [Table 3](#) and [4](#), where  
 1054 for the former table only  $K_f$  showed a high sensitivity effect (close to the value of  
 1055 the baseline test), but as shown in [Table 4](#), when the uncertainty coupling is taken  
 1056 into account for the analysis, then all of the four parameters have similar levels to the

1057 baseline case. This finding results from taking into account perturbations in the other  
 1058 parameters while computing the parameter’s sensitivity, and shows that the coupling  
 1059 among the uncertainties (not captured with first-order sensitivity approaches) can  
 1060 drastically affect the importance of some parameters. Specifically, parameters deemed  
 1061 unimportant with a first-order analysis can instead have a non-negligible impact on  
 1062 the bifurcation point.

1063 To further characterize this aspect, Figure 6 depicts the reciprocal of the robust  
 1064 bifurcation margin  $k_m$  as a function of the frequency. The five curves represent the  
 1065 five cases considered in Table 4 and, unlike the *one-shot* tests discussed therein, are  
 1066 obtained by fixing the frequency in the optimization and computing the value of the  
 margin at each frequency.

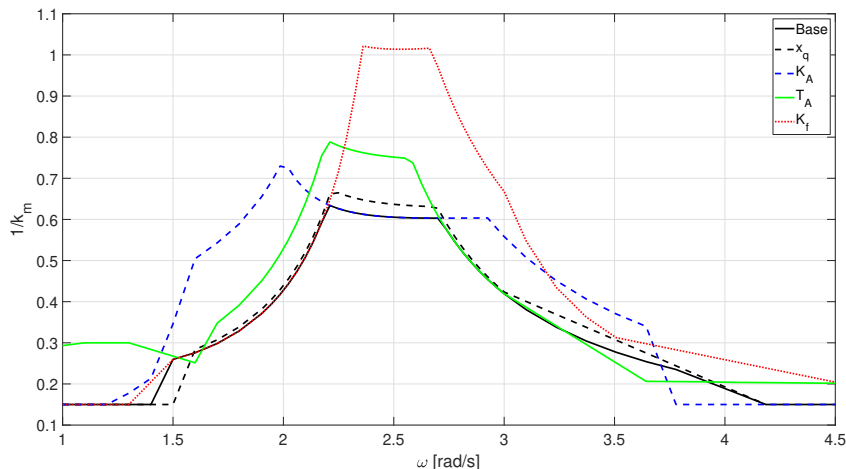


FIG. 6. Sensitivity analysis of four parameters based on the robust bifurcation margin.

1067 The curves in Figure 6 resemble those typically employed in linear robust analysis  
 1068 with  $\mu$  [48, 2, 26]. This points out once again the connection between the proposed  
 1069 concept of robust bifurcation margin  $k_m$  and the structured singular value  $\mu$ . In  
 1070 particular, when  $\frac{1}{k_m} \geq 1$ , a perturbation in the allowed range of uncertainties exists  
 1071 such that a Hopf bifurcation is experienced by the system when perturbed. Note that  
 1072 the peak of each curve coincides with the reciprocal of the margin reported in Table  
 1073 4. This representation allows the different sensitivities to the parameters discussed  
 1074 previously to be immediately inferred.

## 1076 4.2. Aeroelastic system.

1077 **4.2.1. Model description.** The typical section is an aeroelastic case study com-  
 1078 monly used for flutter analysis purposes [4], and consists of a rigid airfoil with lumped  
 1079 springs simulating the 3 structural degrees of freedom (DOFs): plunge  $h$ , pitch  $\alpha$  and  
 1080 trailing edge flap  $\beta$ . By defining the vector of structural states  $x_s = [\frac{h}{b}; \alpha; \beta]$  and  
 1081 aerodynamic states  $x_a$  (used to capture the unsteady aerodynamic contribution), the  
 1082 system can be described in matrix form as:

$$1083 \quad (4.4) \quad \dot{x} = \begin{bmatrix} \dot{x}_s \\ \dot{x}_a \end{bmatrix} = \begin{bmatrix} 0 & I & 0 \\ -M^{-1}K & -M^{-1}B & M^{-1}D \\ 0 & E & R \end{bmatrix} \begin{bmatrix} x_s \\ \dot{x}_s \\ x_a \end{bmatrix} = \mathcal{A}x,$$

1084 where  $M$ ,  $B$  and  $K$  are respectively the aeroelastic inertial, damping and stiffness  
1085 matrices:

$$\begin{aligned}
 M &= M_s - \frac{1}{2}\rho_\infty b^2 A_2, \\
 B &= -\frac{1}{2}\rho_\infty b V A_1, \\
 K &= K_s - \frac{1}{2}\rho_\infty V^2 A_0.
 \end{aligned}
 \tag{4.5}$$

1087 They include the structural mass  $M_s$  and stiffness matrices  $K_s$  plus the aerodynamic  
1088 quasi-steady matrices  $A_i$  ( $\rho_\infty$  is the air density and  $b$  the half chord distance).  $D$ ,  $E$ ,  
1089 and  $R$  in (4.4) come from the rational approximation of the unsteady aerodynamic  
1090 operator. The parameters defining the model are provided in [25] and the total state  
1091 size  $n_x$  is 9 (6 structural and 3 aerodynamic). The interested reader is referred to [25]  
1092 for a complete definition of the parameters defining the model and further details on  
1093 aeroelastic modeling with uncertainties.

1094 Nonlinearities in  $K_s$  are considered in this work. Specifically, hardening cubic  
1095 terms for the plunge and pitch degrees of freedom are assumed, and the matrix  $K_s$  is  
1096 rewritten accordingly:

$$\tag{4.6} K_s = K_s^L + K_s^{NL} = \begin{bmatrix} K_h^L & 0 & 0 \\ 0 & K_\alpha^L & 0 \\ 0 & 0 & K_\beta \end{bmatrix} + \begin{bmatrix} K_h^{NL} K_h^L (\frac{h}{b})^2 & 0 & 0 \\ 0 & K_\alpha^{NL} K_\alpha^L \alpha^2 & 0 \\ 0 & 0 & 0 \end{bmatrix},$$

1098 where  $K_h$ ,  $K_\alpha$  and  $K_\beta$  are respectively the plunge, pitch and control surface stiffness.  
1099 As is common practice [11], the coefficients of the nonlinear terms are assumed pro-  
1100 portional to the corresponding linear ones through the dimensionless coefficients  $K_h^{NL}$   
1101 and  $K_\alpha^{NL}$  (assumed here equal to 100). The hardening effect modelled in (4.6) takes  
1102 into account the fact that the stiffness properties change when the system undergoes  
1103 large deformations, with an increase in the stiffness generally observed.

1104 The dynamics of the system is thus in the form of the generic vector field (2.1),  
1105 and, by selecting the speed  $V$  as bifurcation parameter, it holds:

$$\begin{aligned}
 \dot{x} &= f(x, V) = \mathcal{A}^L(V)x + f^{NL}(x), \\
 J(x, V) &= \mathcal{A}^L(V) + \nabla_x f^{NL}(x),
 \end{aligned}
 \tag{4.7}$$

1107 where:  $\mathcal{A}^L : \mathbb{R} \rightarrow \mathbb{R}^{n_x \times n_x}$  is obtained from  $\mathcal{A}$  (4.4) by setting the nonlinear terms  
1108 to zero;  $f^{NL} : \mathbb{R}^{n_x} \rightarrow \mathbb{R}^{n_x}$  is the nonlinear part of the vector field; and the state is  
1109  $x = [x_s; \dot{x}_s; x_a]$ . Note that, for the nonlinearities considered here (4.6),  $f^{NL}$  (and thus  
1110 also  $\nabla_x f^{NL}$ ) does not depend on the speed.

1111 Following the notation in section 3.1,  $V_H$  will denote the speed at which the  
1112 nominal system undergoes a Hopf bifurcation, and after which it will potentially  
1113 exhibit limit cycle oscillations. Given a subcritical speed  $\bar{V}_0$  (such that  $\bar{V}_0 < V_H$   
1114 corresponds to a stable equilibrium) and the definition of a vector  $\delta$  of parametric  
1115 uncertainties, then the distance in the parameter space of the equilibrium at  $\bar{V}_0$  from  
1116 the closest Hopf bifurcation is computed by means of the robust bifurcation margin  
1117  $k_m$ . The robust bifurcation analysis will thus allow the quantification of the influence  
1118 of parametric uncertainties on the onset of LCO, which are a notorious problem for  
1119 nonlinear aeroelastic systems [11].

1120 Numerical continuation can be applied to (4.7) after having specified the value  
1121 of the trim state  $x_t$ . Two cases will be considered, case 1 ( $c_1$ ) with  $x_t = 0$  and case

1122 2 (*c2*) featuring a non-zero value  $\alpha_t = 1^\circ$  for the angle of attack of the section. The  
 1123 latter is physically motivated by the fact that the section is generating positive lift to  
 1124 counterbalance gravitational forces directed downwards. Figure 7 shows the standard  
 1125 (i.e. nominal) bifurcation diagrams with  $V$  on the  $x$ -axis and the normalized plunge  
 1126 DOF  $\frac{h}{b}$  on the  $y$ -axis (in the case of branches of LCO solution branches, this is the  
 1127 maximum value over a period). The usual convention of representing stable steady-  
 1128 states (equilibria and LCOs) with solid lines and unstable ones with dashed lines is  
 1129 adopted, and the Hopf bifurcation is marked with a circle.

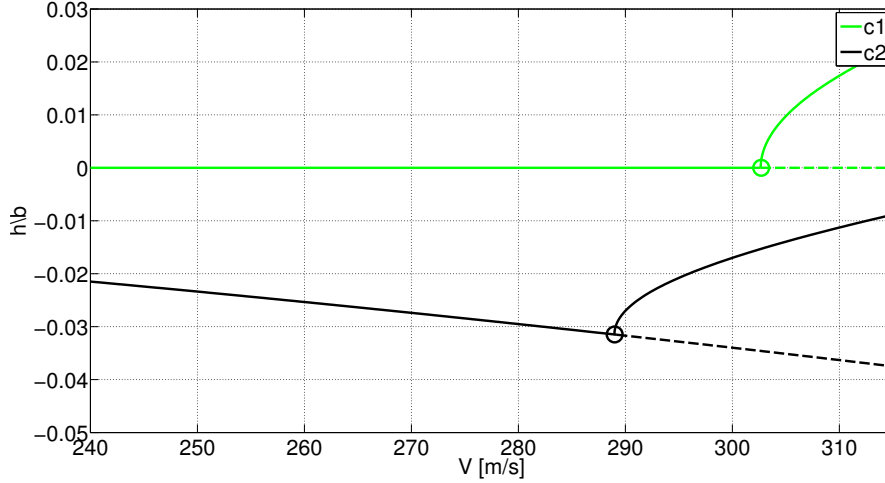


FIG. 7. Bifurcation diagram for the nominal vector field for two different trim states.

1130 The system experiences supercritical Hopf bifurcations at  
 1131  $V_H = 302.7 \frac{m}{s}$  for *c1* and  $V_H = 289.0 \frac{m}{s}$  for *c2*. The frequency of the associated  
 1132 imaginary eigenvalues are respectively  $\omega_H = 70 \frac{rad}{s}$  and  $\omega_H = 75 \frac{rad}{s}$ .

1133 **4.2.2. Computation of robust bifurcation margins.** Including uncertainties  
 1134 in the nominal vector field of (4.7) yields the expression for the uncertain vector field  
 1135

$$1136 \quad (4.8a) \quad \dot{x} = \tilde{f}(x, V, \delta) = \tilde{A}^L(V, \delta)x + \tilde{f}^{NL}(x, V, \delta),$$

$$1137 \quad (4.8b) \quad \tilde{J}(x, V, \delta) = \tilde{A}^L(V, \delta) + \nabla_x \tilde{f}^{NL}(x, V, \delta).$$

1139 The bifurcation parameter  $V$  will be fixed in the subsequent analyses to  $\bar{V}_0 = 270 \frac{m}{s}$ ,  
 1140 which, recall Figure 7, is associated in both cases with stable equilibria –and hence,  
 1141 it is a valid choice according to the discussion in section 3.1.

1142 The initial step to compute robust bifurcation margins is the definition of the  
 1143 nominal system and of the uncertainty set, which in turn will drive the construction of  
 1144 the underlying LFT. The former is described by (4.7), while the uncertainty definition  
 1145 is chosen to define a range of variation of  $\pm 10\%$  from the nominal value for the  
 1146 coefficients  $M_{s_{11}}$ ,  $M_{s_{22}}$ ,  $K_{s_{22}}$  and of  $\pm 5\%$  for  $M_{s_{12}}$  and  $K_{s_{11}}$

$$1147 \quad (4.9) \quad \Delta_u = \text{diag}(\delta_{K_{s_{22}}^L}, \delta_{K_{s_{11}}^L}, \delta_{M_{s_{11}}}, \delta_{M_{s_{12}}}, \delta_{M_{s_{22}}}).$$

1148 This uncertainty definition was considered since it is the same as that used in [25],  
 1149 where the linear problem (i.e.  $K_h^{NL} = K_\alpha^{NL} = 0$ ) was extensively analyzed by means

1150 of nominal (eigenvalue analysis) and robust ( $\mu$  analysis) techniques. This testcase is  
 1151 thus used to benchmark the first set of numerical results obtained with the method  
 1152 proposed in this paper.

1153 **Program 3.2** is computed with an initialization provided by the nominal values of  
 1154 the equilibrium point and of the uncertainties. The results from the program are re-  
 1155 ported in Table 5 in terms of robust stability margin  $k_m$ , frequency  $\hat{\omega}$  of the imaginary  
 1156 eigenvalues at  $\bar{V}_0$ , and type of Hopf bifurcation. Recall indeed that **Program 3.2** cal-  
 1157 culates the closest Hopf bifurcation without constraining the value of  $l_1$ , and the type  
 1158 of predicted Hopf bifurcation was assessed a posteriori with numerical continuation  
 of the perturbed system.

TABLE 5  
 Robust bifurcation margins at  $\bar{V}_0 = 270 \frac{m}{s}$  for uncertainties in the set (4.9).

|    | $k_m$ | $\hat{\omega} \frac{rad}{s}$ | type  |
|----|-------|------------------------------|-------|
| c1 | 0.73  | 71.5                         | super |
| c2 | 0.49  | 75.1                         | super |

1159  
 1160 It is inferred from the first column of Table 5 that in both cases the Hopf bifur-  
 1161 cation could be shifted to  $V = 270 \frac{m}{s}$  within the uncertainty range (note indeed that  
 1162  $k_m < 1$ ). Another important observation is that c1 gives a margin  $k_m$  within less  
 1163 than 1% of the result from the literature [25] (obtained with  $\mu$  considering the linear  
 1164 system at the same speed  $V = 270 \frac{m}{s}$ ). The (normalized) uncertainty vector found  
 1165 here by the optimizer is

$$\begin{aligned}
 1166 \quad (4.10) \quad \hat{\delta} &= [\delta_{K_{s22}^L}; \delta_{K_{s11}^L}; \delta_{M_{s11}}; \delta_{M_{s12}}; \delta_{M_{s22}}], \\
 &= [-0.7328; 0.7328; -0.7328; 0.5027; 0.7328],
 \end{aligned}$$

1167 which also features the same perturbations (within a small tolerance) as those de-  
 1168 tected in [25] (their physical meaning in relation to the onset of flutter was discussed  
 1169 in the reference). In order to better appreciate the importance of this result, let  
 1170 us recall that nominal analyses (Figure 7) found for c1 the branch of equilibria at  
 1171  $x = 0$  regardless of  $V$ . Since the uncertainties selected here only affect  $\tilde{\mathcal{A}}^L$ , then  
 1172  $\tilde{f}^{NL}(0, V, \cdot) = f^{NL}(0, V) = 0$  and thus  $\nabla_x \tilde{f}^{NL} \equiv 0$ . That is, the determination of  
 1173  $k_m$  is equivalent (for this specific case) to the problem solved by  $\mu$ , i.e., finding the  
 1174 smallest perturbation matrix such that  $\tilde{\mathcal{A}}^L$  is neutrally stable. The good matching  
 1175 with the literature results is very important, since in [25]  $\mu_{LB}$  and  $\mu_{UB}$  were shown  
 1176 to be close, indicating that the true value of  $\mu$  was determined. This result hence ver-  
 1177 ifies the correctness of the approach proposed here since it recovers the result which,  
 1178 for this specific case, is known a priori to be the correct one. Moreover, at least for  
 1179 this case, **Program 3.2** is able to detect the global minimum of the optimization.

1180 Another positive feature is that **Program 3.2** has the frequency  $\omega$  as a decision vari-  
 1181 able, whereas  $\mu$  was applied in [25] at discrete frequencies because this is the available  
 1182 implementation for the standard algorithms [2] (which has the drawback of possibly  
 1183 missing critical frequencies and thus overestimating the value of the stability margin).

1184 Case c2 is then considered (with  $\alpha_t = 1^\circ$ ). This cannot be analyzed with  $\mu$   
 1185 because  $\tilde{J}$  is now also a function of the nonlinear terms due to non zero values for  
 1186 the equilibria (which in turn depend on the uncertainty). For this reason, it is not  
 1187 possible to compare the results with the true analytic solution. However, it is noted  
 1188 that  $k_m$  now achieves a smaller value than for c1. This is in accordance with the  
 1189 nominal analyses in Figure 7, for which c2 presented a smaller  $V_H$  than c1. Thus,

1190 as  $\bar{V} = 270 \frac{m}{s}$  is closer to the nominal bifurcation speed for  $c2$ , a smaller robustness  
 1191 margin is expected. Note also that the two predicted frequencies  $\hat{\omega}$  are relatively close  
 1192 to the nominal ones. These interpretations thus give some confidence that an accurate  
 1193 prediction of the margin has also been obtained for  $c2$ .

1194 Other important information gathered in Table 5 is the type of closest Hopf bi-  
 1195 furcations. Note that in order to obtain this result, the solver COCO was used to  
 1196 perform numerical continuation of the perturbed system, which also allowed verifi-  
 1197 cation that the latter experienced a Hopf bifurcation at  $\bar{V}_0 = 270 \frac{m}{s}$ , as expected.  
 1198 These analyses show that the closest Hopf bifurcations are of the same nature as the  
 1199 corresponding ones in nominal conditions. Based on the greater attention typically  
 1200 devoted to subcritical LCOs due to the associated risks [11], the following analyses  
 1201 will make use of Program 3.4 to investigate whether changes in parameter values can  
 1202 drive the Hopf bifurcation from supercritical to subcritical. Without loss of generality,  
 1203 only the case  $c2$  will be considered.

1204 Uncertainties in two aerodynamic parameters are added to the set (4.9), namely,  
 1205 the terms  $A_{012}$  and  $A_{022}$  of the steady aerodynamics matrix  $A_0$  (4.5). These corre-  
 1206 spond to the lift and moment coefficients of the airfoil respectively, and are allowed  
 1207 to vary within  $\pm 20\%$  from their nominal values. Table 6 shows the solutions provided  
 1208 by Program 3.4 for the two types of possible Hopf bifurcation in terms of: Lyapunov  
 1209 coefficient  $l_1$ , stability margin  $k_m$ , frequency  $\hat{\omega}$ , and normalized perturbations. A  
 tolerance  $\epsilon_l = 1$  on the value of the Lyapunov coefficient was used.

TABLE 6  
 Worst-case perturbations and margins to supercritical and subcritical Hopf bifurcations.

|       | $l_1$   | $k_m$ | $\hat{\omega} \frac{rad}{s}$ | $\delta_{K_{s22}^L}$ | $\delta_{K_{s11}^L}$ | $\delta_{M_{s11}}$ | $\delta_{M_{s12}}$ | $\delta_{M_{s22}}$ | $\delta_{A_{022}}$ | $\delta_{A_{012}}$ |
|-------|---------|-------|------------------------------|----------------------|----------------------|--------------------|--------------------|--------------------|--------------------|--------------------|
| super | $-10^3$ | 0.25  | 76                           | -0.25                | 0.25                 | -0.25              | -0.25              | 0.25               | 0.25               | -0.25              |
| sub   | 1       | 3.13  | 67                           | -3.12                | 3.12                 | -3.12              | -3.12              | 3.12               | 3.12               | 1.83               |

1210 The supercritical case is consistent with the corresponding case in Table 5. Indeed,  
 1211 the margin approximatively halves as a result of the additional uncertainty in the  
 1212 system, while the frequency has a similar value. Note also that the constraint on  $l_1$   
 1213 is not active and thus  $l_1$  has a large absolute value. On the contrary, the subcritical  
 1214 case features a far higher margin (which, according to the definition of  $k_m$  given in  
 1215 subsection 3.1, points out that there is no perturbation inside the allowed set capable  
 1216 of prompting the investigated bifurcation) and achieves a value of  $l_1$  equal to the  
 1217 tolerance  $\epsilon_l$ . Another interesting fact is that while all the normalized perturbations  
 1218 feature the same sign as in the supercritical case, this does not hold for  $A_{012}$  which  
 1219 has an opposite perturbation and, in absolute value, smaller than the others. This  
 1220 is an interesting aspect, because according to standard interpretations of unstable  
 1221 aeroelastic phenomena [4, 25], a negative perturbation for  $A_{012}$  would be expected  
 1222 (as noted for the supercritical case). The justification for this could be sought in  
 1223 the physical mechanisms prompting subcritical LCO [11] and will be investigated in  
 1224 future studies. It is remarked here that the commented scenario is distinctive of  
 1225 this problem, where different (possibly conflicting) constraints define the worst-case  
 1226 conditions. While robustness in the linear context focuses on the loss of stability  
 1227 only, from a dynamical systems perspective this becomes a multi-faceted concept  
 1228 characterized by concurrent conditions and thus non-intuitive results can be found.

1230 Figure 8 shows bifurcation diagrams relative to worst-case combinations of pa-  
 1231 rameters found by Program 3.4 by changing the tolerance on the Lyapunov coefficient



1232  $\epsilon_l$ . In the legend of Figure 8, the value of the Lyapunov coefficient at the bifurcation  
 1233 point is indicated.

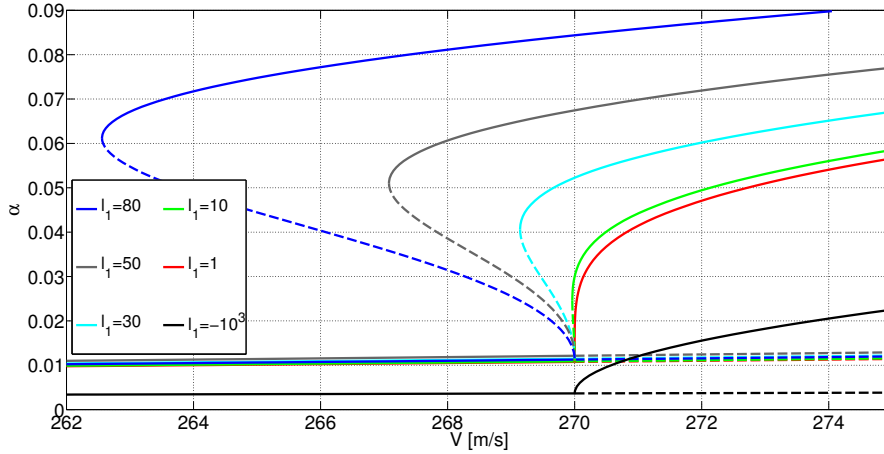


FIG. 8. Bifurcation diagram of the system for different worst-case perturbations.

1233

1234

1235

1236

1237

1238

1239

1240

1241

1242

1243

1244

1245

1246

1247

1248

1249

1250

1251

1252

1253

1254

1255

1256

1257

1258

1259

1260

1261

1262

1263

The first important observation is that all the cases display a Hopf bifurcation at  $\bar{V}_0 = 270 \frac{m}{s}$ . The branches relative to the solutions from Table 6 (obtained with  $\epsilon_l = 1$ ) are  $l_1 = -10^3$  and  $l_1 = 1$ . This in turn demonstrates that Program 3.4 is able to correctly predict worst-case combinations of uncertainty which lead to respectively supercritical and subcritical bifurcation. For the other curves  $l_1 = \epsilon_l$  holds since this constraint is always active, and the associated margins  $k_m$  slightly increase compared to the value 3.13 featured in Table 6. It is stressed that a quantitative interpretation of the absolute value of  $l_1$  depends on the arbitrary normalization adopted for the eigenvector  $q$  in its definition (3.10). The point made here is qualitative and, specifically, is that as the tolerance  $\epsilon_l$  (and thus  $l_1$ ) is increased, the subcritical Hopf bifurcation predicted by the optimizer is more pronounced (i.e. the range of speeds for which unstable and stable LCOs coexist with the branch of stable equilibria is larger). Even though this is not guaranteed by the Hopf bifurcation theorem, since  $l_1$  is defined on the center manifold at the bifurcation point only, the magnitude of the Lyapunov coefficient can be taken as a measure of the subcriticality of the LCO (when comparing different instances computed with the same normalization of  $q$ ). Figure 8 shows therefore that embedding the constraint on the Lyapunov coefficient in the bifurcation margin computation is successfully done by the optimization.

The last part of the section is aimed at providing insights into the numerical aspects of the algorithms. As a preamble, it is observed that there are not definitive answers with respect to robustness to local minima or efficiency of the algorithms as these will depend on many aspects such as, for example, the type of vector field (not only size and degree, but also number of attractors) and the optimization algorithm employed (which is an aspect that has not been investigated in this work). Investigation of these important features are left for future work.

The execution time of Program 3.4 is larger than that of Program 3.2 (approximately 6s against 3s for the case with 7 uncertainties). Most importantly, the addition of the constraint on  $l_1$  exacerbates the issue of local minima, especially when this is an active constraint. The set of strategies described in Section 3.3 were thus employed to obtain the results presented in Figure 8. Specifically, reinitializing the optimization

1264 with points on the auxiliary manifold  $\mathcal{H}_g$  and with solutions obtained by fixing the  
 1265 frequency in [Program 3.4](#) led to significant improvements in the solution.

1266 Finally, it is remarked that for all the analyzed cases, the worst-case combina-  
 1267 tions of the uncertain parameters predicted by the optimization problem were used to  
 1268 perform numerical continuation analyses of the perturbed system with COCO. In all  
 1269 cases the perturbed systems encountered a Hopf bifurcation at the pre-selected speed  
 1270  $\bar{V}_0$ . Even though this fact does not ensure that the global optimum (i.e. smallest  
 1271 margin to bifurcation) was found, it represents important evidence of the validity of  
 1272 the overall approach.

1273 **5. Conclusions.** The paper develops a framework for the analysis of nonlinear  
 1274 systems subject to parametric uncertainties with the goal of studying robustness of  
 1275 stable equilibria to the onset of dynamic bifurcations. A scalar metric quantifying a  
 1276 perturbation in the uncertainty set is first defined, and the magnitude of the smallest  
 1277 perturbation such that a stable equilibrium is driven into a Hopf bifurcation point is  
 1278 named the robust bifurcation margin  $k_m$ . Its definition, which also allows the nature  
 1279 of the closest Hopf bifurcation (subcritical or supercritical) to be specified, is based  
 1280 on the idea of building a Linear Fractional Transformation model of the uncertain  
 1281 Jacobian and studying its singularity. The proposed margin can be interpreted as an  
 1282 extension of the structured singular value  $\mu$  to the nonlinear context. The compu-  
 1283 tation of  $k_m$  is recast as a nonlinear smooth constrained optimization problem, and  
 1284 as such it suffers in principle from the issue of local minima. Thus, the proposed  
 1285 programs technically provide only an upper bound on the margin. However, several  
 1286 mitigation strategies are described in order to tighten the gap with the actual margin,  
 1287 including a continuation-based multi-start strategy. Application of the framework is  
 1288 demonstrated on two case studies: a power system model and an aeroelastic system  
 1289 exhibiting nonlinear flutter behaviour. For the former, analyses show that  $k_m$  can be  
 1290 used to infer sensitivity of the Hopf bifurcation to system's parameters and it allows  
 1291 more accurate predictions than those achieved with available methods only providing  
 1292 first-order information. As for the latter, first the same results obtained in the lit-  
 1293 erature with  $\mu$  are retrieved, and then the possibility to distinguish between closest  
 1294 subcritical and supercritical bifurcations is explored. The results verify from different  
 1295 perspectives soundness of the newly introduced concept and provide examples of its  
 1296 perspective advantages over available techniques to study the nonlinear robustness  
 1297 problem in different application domains.

1298

## REFERENCES

- 1299 [1] G. B. ARFKEN AND H. J. WEBER, *Mathematical methods for physicists*, Academic Press; 4th  
 1300 ed., San Diego, CA, 1995.
- 1301 [2] G. BALAS, R. CHIANG, A. PACKARD, AND M. SAFONOV, *Robust Control Toolbox*, 2009.
- 1302 [3] W. BEYN, A. CHAMPNEYS, E. DOEDEL, W. GOVAERTS, Y. A. KUZNETSOV, AND B. SANDSTEDE,  
 1303 *Numerical continuation, and computation of normal forms.*, in Handbook of Dynamical  
 1304 Systems, Vol 2 / B. Fiedler (edit.), Elsevier, 2002, Chapter 4. - ISBN 0-444-50168-1, 2002,  
 1305 pp. 149–219.
- 1306 [4] R. L. BISPLINGHOFF AND H. ASHLEY, *Principles of Aeroelasticity*, Wiley, 1962.
- 1307 [5] R. BRAATZ, P. YOUNG, J. DOYLE, AND M. MORARI, *Computational-complexity of  $\mu$ -calculation*,  
 1308 IEEE Transactions on Automatic Control, 39 (1994), pp. 1000–1002.
- 1309 [6] C. A. CANIZARES, *Calculating optimal system parameters to maximize the distance to saddle-*  
 1310 *node bifurcations*, IEEE Transactions on Circuits and Systems, 45 (1998), pp. 225–237.
- 1311 [7] J. H. CHOW AND A. GEBRESELASSIE, *Dynamic voltage stability analysis of a single machine*  
 1312 *constant power load system*, in 29th IEEE Conference on Decision and Control, 1990.
- 1313 [8] G. CIRILLO, G. HABIB, G. KERSCHEN, AND R. SEPULCHRE, *Analysis and design of nonlinear*

- 1314 *resonances via singularity theory*, Journal of Sound and Vibration, 392 (2017), pp. 295–306.
- 1315 [9] H. DANKOWICZ AND F. SCHILDER, *An extended continuation problem for bifurcation analysis*
- 1316 *in the presence of constraints*, ASME 2009 International Design Engineering Technical
- 1317 *Conferences and Computers and Information in Engineering Conference*, 2009.
- 1318 [10] H. DANKOWICZ AND F. SCHILDER, *Recipes for Continuation*, Society for Industrial and Applied
- 1319 *Mathematics*, Philadelphia, PA, 2013.
- 1320 [11] G. DIMITRIADIS, *Introduction to Nonlinear Aeroelasticity*, Aerospace Series, Wiley, 2017.
- 1321 [12] I. DOBSON, *Computing a closest bifurcation instability in multidimensional parameter space*,
- 1322 *Journal of Nonlinear Science*, 3 (1993), pp. 307–327.
- 1323 [13] I. DOBSON, F. ALVARADO, AND C. L. DEMARCO, *Sensitivity of hopf bifurcations to power*
- 1324 *system parameters*, in [1992] *Proceedings of the 31st IEEE Conference on Decision and*
- 1325 *Control*, 1992.
- 1326 [14] E. J. DOEDEL, T. F. FAIRGRIEVE, B. SANDSTED, A. R. CHAMPNEYS, Y. A. KUZNETSOV,
- 1327 *AND X. WANG*, *Auto-07p: Continuation and bifurcation software for ordinary differential*
- 1328 *equations*, tech. report, 2007.
- 1329 [15] J. DOYLE, *Analysis of feedback systems with structured uncertainties*, IEE Proceedings D Con-
- 1330 *trol Theory and Applications*, 129 (1982), pp. 242–250.
- 1331 [16] J. GERHARD, W. MARQUARDT, AND M. MONNIGMANN, *Normal vectors on critical manifolds*
- 1332 *for robust design of transient processes in the presence of fast disturbances*, SIAM Journal
- 1333 *on Applied Dynamical Systems*, 7 (2008), pp. 461–490.
- 1334 [17] P. GILL, W. MURRAY, AND M. WRIGHT, *Practical optimization*, Academic Press, 1981.
- 1335 [18] M. GOLUBITSKY AND D. SCHAEFFER, *Singularities and Groups in Bifurcation Theory*, Applied
- 1336 *Mathematical Sciences*, Springer-Verlag New York, 1985.
- 1337 [19] W. GOVAERTS, *Numerical Methods for Bifurcations of Dynamical Equilibria*, Society for In-
- 1338 *dustrial and Applied Mathematics*, 2000.
- 1339 [20] R. GRAY, A. FRANCI, V. SRIVASTAVA, AND N. E. LEONARD, *Multiagent decision-making dy-*
- 1340 *namics inspired by honeybees*, IEEE Transactions on Control of Network Systems, 5 (2018),
- 1341 *pp. 793–806*.
- 1342 [21] J. GUCKENHEIMER AND P. HOLMES, *Nonlinear Oscillations, Dynamical Systems, and Bifurca-*
- 1343 *tions of Vector Fields*, Applied Mathematical Sciences, Springer New York, 2002.
- 1344 [22] M. HAYES, D. BATES, AND I. POSTLETHWAITE, *New tools for computing tight bounds on the*
- 1345 *real structured singular value*, Journal of Guidance, Control, and Dynamics, 24 (2001),
- 1346 *pp. 1204–1213*.
- 1347 [23] R. HORN AND C. JOHNSON, *Matrix Analysis*, Cambridge University Press, 1990.
- 1348 [24] A. IANNELLI, M. LOWENBERG, AND A. MARCOS, *An extension of the structured singular value*
- 1349 *to nonlinear systems with application to robust flutter analysis*, 5th CEAS Conference on
- 1350 *Guidance, Navigation and Control (EuroGNC)*, 2019.
- 1351 [25] A. IANNELLI, A. MARCOS, AND M. LOWENBERG, *Aeroelastic modeling and stability analysis:*
- 1352 *A robust approach to the flutter problem*, International Journal of Robust and Nonlinear
- 1353 *Control*, 28 (2018), pp. 342–364.
- 1354 [26] A. IANNELLI, A. MARCOS, AND M. LOWENBERG, *Study of Flexible Aircraft Body Freedom Flutter*
- 1355 *with Robustness Tools*, J. of Guidance, Control and Dynamics, 41 (2018), pp. 1083–1094.
- 1356 [27] Y. KUZNETSOV, *Elements of Applied Bifurcation Theory*, Springer-Verlag New York, 2004.
- 1357 [28] J. MAGNI, *Linear fractional representation toolbox modelling, order reduction, gain scheduling*,
- 1358 *Technical Report TR 6/08162*, DCSD, ONERA, Systems Control and Flight Dynamics
- 1359 *Department*, 2004.
- 1360 [29] A. MARCOS, D. BATES, AND I. POSTLETHWAITE, *Nonlinear symbolic LFT tools for modeling,*
- 1361 *analysis and design*, in *Nonlinear Analysis and Synthesis Techniques in Aircraft Control*,
- 1362 *L. N. in Control and S.-V. Information Science*, eds., 2007.
- 1363 [30] A. MARCOS, D. BATES, AND I. POSTLEWHITE, *Control oriented uncertainty modeling using*
- 1364  *$\mu$  sensitivities and skewed  $\mu$  analysis tool*, in *IEEE Conference on Decision and Control*,
- 1365 *2005*.
- 1366 [31] MATLAB, *Optimization Toolbox User’s Guide*, 2014.
- 1367 [32] A. MAZZOLENI AND I. DOBSON, *Closest bifurcation analysis and robust stability design of flexible*
- 1368 *satellites*, Journal of Guidance, Control, and Dynamics, 18 (1995), pp. 333–339.
- 1369 [33] Z. MICHALEWICZ AND D. FOGEL, *How to Solve It: Modern Heuristics*, Springer-Verlag, 2nd ed.,
- 1370 *2004*.
- 1371 [34] M. MONNIGMANN AND W. MARQUARDT, *Steady-state process optimization with guaranteed ro-*
- 1372 *burst stability and feasibility*, AIChE Journal, 49, pp. 3110–3126.
- 1373 [35] A. PACKARD AND J. DOYLE, *The Complex Structured Singular Value*, Automatica, 29 (1993),
- 1374 *pp. pp. 71–109*.
- 1375 [36] A. PACKARD, M. FAN, AND J. DOYLE, *A power method for the structured singular value*, Proc.

- 1376 of the Conference on Decision and Control, December 1988.
- 1377 [37] A. ROBERTS, *Computer algebra derives correct initial conditions for low-dimensional dynamical*  
1378 *models*, Computer Physics Communications, 126 (2000), pp. 187 – 206.
- 1379 [38] A. ROBERTS, *Normal form transforms separate slow and fast modes in stochastic dynamical*  
1380 *systems*, Physica A: Statistical Mechanics and its Applications, 387 (2008), pp. 12 – 38.
- 1381 [39] C. ROOS, *Systems modeling, analysis and control (SMAC) toolbox: An insight into the robust-*  
1382 *ness analysis library*, in 2013 IEEE Conference on Computer Aided Control System Design  
1383 (CACSD), 2013.
- 1384 [40] C. ROOS AND J. BIANNIC, *A detailed comparative analysis of all practical algorithms to compute*  
1385 *lower bounds on the structured singular value*, Control Engineering Practice, 44 (2015),  
1386 pp. 219–230.
- 1387 [41] W. D. ROSEHART AND C. A. CANIZARES, *Bifurcation analysis of various power system models*,  
1388 International Journal of Electrical Power & Energy Systems, 21 (1999), pp. 171 – 182.
- 1389 [42] M. SAFONOV, *Origins of robust control: Early history and future speculations*, 7th IFAC Sym-  
1390 *posium on Robust Control Design*, June 2012.
- 1391 [43] M. SAFONOV AND M. ATHANS, *A multiloop generalization of the circle criterion for stability*  
1392 *margin analysis*, IEEE Transactions on Automatic Control, 26 (1981), pp. 415–422.
- 1393 [44] P. SEILER, A. PACKARD, AND G. J. BALAS, *A gain-based lower bound algorithm for real and*  
1394 *mixed  $\mu$  problems*, Automatica, 46 (2010), pp. 493–500.
- 1395 [45] A. TAYLOR AND W. MANN, *Advanced Calculus*, Wiley, 1983.
- 1396 [46] V. VENKATASUBRAMANIAN, H. SCHATTLER, AND J. ZABORSZKY, *Voltage dynamics: study of a*  
1397 *generator with voltage control, transmission, and matched MW load*, IEEE Transactions  
1398 on Automatic Control, 37 (1992), pp. 1717–1733.
- 1399 [47] A. YAZICI, A. KARAMANCIOĞLU, AND R. KASIMBEYLI, *A nonlinear programming technique*  
1400 *to compute a tight lower bound for the real structured singular value*, Optimization and  
1401 Engineering, 12 (2011), pp. 445–458.
- 1402 [48] K. ZHOU, J. C. DOYLE, AND K. GLOVER, *Robust and Optimal Control*, Prentice-Hall, 1996.